AD-A057 642 ILLINOIS UNIV AT URBANA-CHAMPAIGN COORDINATED SCIENCE LAB F/G 9/3
DESIGN OF SAW FILTERS WITH DIFFRACTION COMPENSATION.(U)
FEB 78 S DATTA DAAB07-72-C-0259
UNCLASSIFIED R-809 NL

| OF |
AD
A057642

END
DATE
FILMED
9-78
DDC

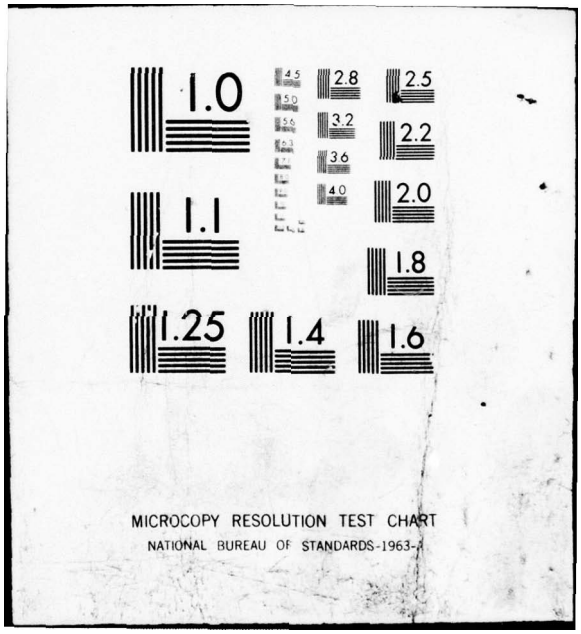
1.0
1.1
1.25
1.4
1.6
1.8
2.0
2.2
2.5
2.8
3.2
3.6
4.0
4.5
5.0
MICROCOPY RESOLUTION TEST CHART
NATIONAL BUREAU OF STANDARDS-1963-A

LEVEL II

REPORT R-809 FEBRUARY, 1978 UILU-ENG 78-2202

CSL COORDINATED SCIENCE LABORATORY

DESIGN OF SAW FILTERS WITH DIFFRACTION COMPENSATION

SUPRIYO DATTA

UNIVERSITY OF ILLINOIS - URBANA, ILLINOIS

UNCLASSIFIED

SECURITY CLASSIFICATION OF THIS PAGE (When Data Entered)

REPORT DOCUMENTATION PAGE

READ INSTRUCTIONS BEFORE COMPLETING FORM

1. REPORT NUMBER

2. GOVT ACCESSION NO.

3. RECIPIENT'S CATALOG NUMBER

4. TITLE (and Subtitle)

DESIGN OF SAW FILTERS WITH DIFFRACTION COMPENSATION.

5. TYPE OF REPORT & PERIOD COVERED

Technical Report

6. PERFORMING ORG. REPORT NUMBER

R-809, UILU-ENG-78-2202

7. AUTHOR(s)

Supriyo Datta

8. CONTRACT OR GRANT NUMBER(s)

DAAB-07-72-C-0259,
F33615-75-C-1291

9. PERFORMING ORGANIZATION NAME AND ADDRESS

Coordinated Science Laboratory
University of Illinois at Urbana-Champaign
Urbana, Illinois 61801

10. PROGRAM ELEMENT, PROJECT, TASK AREA & WORK UNIT NUMBERS

11. CONTROLLING OFFICE NAME AND ADDRESS

Joint Services Electronics Program

12. REPORT DATE

February 1978

13. NUMBER OF PAGES

72

14. MONITORING AGENCY NAME & ADDRESS(if different from Controlling Office)

Master's thesis, 81p.

15. SECURITY CLASS. (of this report)

UNCLASSIFIED

15a. DECLASSIFICATION/DOWNGRADING SCHEDULE

16. DISTRIBUTION STATEMENT (of this Report)

Approved for public release; distribution unlimited

17. DISTRIBUTION STATEMENT (of the abstract entered in Block 20, if different from Report)

18. SUPPLEMENTARY NOTES

19. KEY WORDS (Continue on reverse side if necessary and identify by block number)

Surface Acoustic Wave Filters
Diffraction Analysis
Diffraction-Compensated Design
Cascaded Filters

20. ABSTRACT (Continue on reverse side if necessary and identify by block number)

Surface Acoustic Wave (SAW) devices provide a convenient hardware implementation for non-recursive transversal filters. Because of their low-cost and small size, SAW filters are becoming increasingly popular in various signal processing applications.

DD FORM 1 JAN 73 1473 EDITION OF 1 NOV 65 IS OBSOLETE

UNCLASSIFIED

SECURITY CLASSIFICATION OF THIS PAGE (When Data Entered)

LEVEL II

12

UILU-ENG 78-2202

DESIGN OF SAW FILTERS WITH DIFFRACTION COMPENSATION

by

Supriyo Datta

This work was supported in part by the Joint Services Electronics Program (U.S. Army, U.S. Navy and U.S. Air Force) under Contract DAAB-07-72-C-0259 and in part by the United States Air Force under Contract F33615-75-C-1291.

DESIGN OF SAW FILTERS WITH DIFFRACTION COMPENSATION

BY

SUPRIYO DATTA

B.Tech., Indian Institute of Technology, Kharagpur, 1975

THESIS

Submitted in partial fulfillment of the requirements
for the degree of Master of Science in Electrical Engineering
in the Graduate College of the
University of Illinois at Urbana-Champaign, 1977

Thesis Adviser: Professor B. J. Hunsinger

Urbana, Illinois

ACKNOWLEDGEMENT

I would like to thank Professor Bill J. Hunsinger for his suggestions, assistance and friendship during the preparation of this thesis. I would also like to thank Steve Wilkus for his help in fabricating the devices.

TABLE OF CONTENTS

LIST OF FIGURES

INTRODUCTION

Surface Acoustic Wave (SAW) devices provide a convenient hardware implementation for non-recursive transversal filters. Because of their low-cost and small size, SAW filters are becoming increasingly popular in various signal processing applications.

A transversal filter consists of a tapped delay line (Figure 1a) where the output is obtained as a weighted sum of present and past inputs. A typical SAW filter structure is shown in Figure 1b. In response to an input signal the transmitter generates surface waves that propagate towards the receiver. The acoustic propagation path constitutes the delay line and the set of receiving elements tap the wave at different points along the path. The summation is performed automatically by the bus bar connecting the receiving elements, thus providing a compact realization of the transversal filter concept.

In a practical SAW device there are various second-order effects that degrade the filter performance expected from the idealized model discussed above. Diffraction is among the most important of these effects. The idealized model assumes a plane uniform wavefront for the surface waves. The curvature of the actual wavefront (because of finite transmitter width) thus gives rise to errors in the weight and delays of the taps causing lower selectivity and rejection.

The mathematics of surface wave diffraction on anisotropic crystals is well understood and experimentally verified [9-17]. The effect of diffraction on the frequency response of filters has been

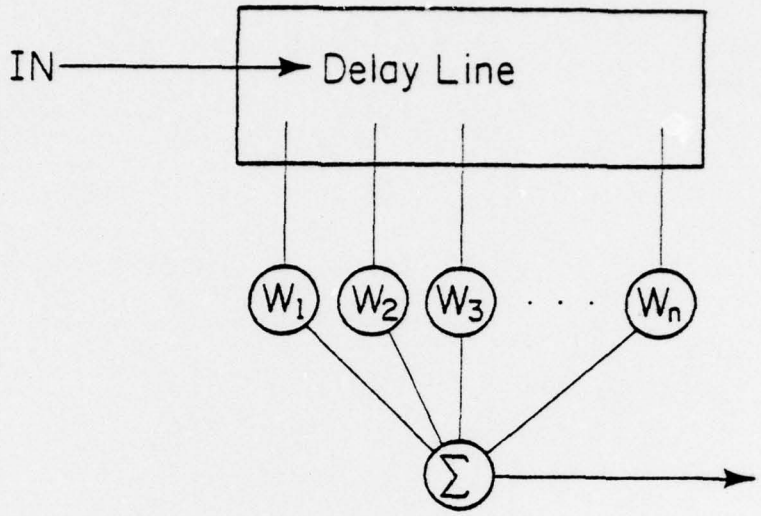

(a)

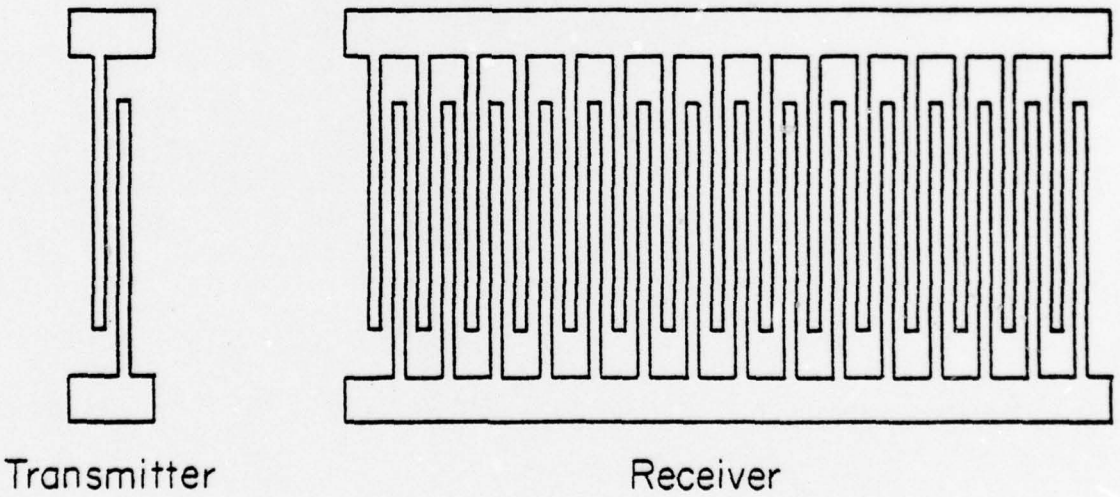

(b)

Figure 1. SAW implementation of non-recursive transversal filters.
(a) Non-recursive transversal filter model
(b) Typical SAW filter structure

analyzed and experimentally verified [6-8,18,19]. However, it has been difficult to model diffraction into a practical design procedure because of the large amount of computation involved. Significant improvement in performance by appropriate diffraction compensation has not been possible in practice.

We have developed an approximate approach to diffraction analysis that reduces calculations by at least an order of magnitude. This approach is particularly significant because its basic assumption is that each tap has a constant strength and delay independent of frequency, which is precisely the assumption one makes in the design of surface acoustic wave devices. The error in this approach is thus an error that cannot be corrected by present tap weighting techniques no matter how accurate the analysis might be. The effect of these errors has been investigated on different types of filters. A real-time design procedure with diffraction correction has been developed on the basis of this approach. Also a new technique has been proposed and verified for implementing the tap weight and delay corrections.

Chapter I describes the analysis technique and its experimental verification. Chapter II describes the procedure for diffraction correction and its limitations. It also describes a practical implementation of the correction technique. The discussion in this chapter is limited to single filters (only one transducer is weighted, the other being short and uniform). Chapter III discusses methods for diffraction corrected design of cascaded filters. The analysis and design is presented with reference to materials

like ST quartz with a parabolic velocity surface. The problem with non-parabolic substrates is one of computational complexity and inaccurate knowledge of velocities [9] and is not discussed further.

CHAPTER I: DIFFRACTION ANALYSIS

In this chapter the theory of surface wave diffraction as applied to interdigital transducers is discussed. It also describes the application of this theory to predict the performance of actual devices and experimental confirmation of the predictions.

1. Tap Weighting Techniques Based on a No-diffraction Model

This section briefly discusses the different techniques used to implement tap weighting since diffraction effects depend strongly on the particular technique used.

SAW filters are commonly modeled as ideal delay lines assuming a Fourier transform relationship between the tap weights and the device frequency response. The specified transfer function H(f) is inverse Fourier transformed and sampled to yield the tap weights $W(t_n)$ such that [1,2],

$$H(f) = \sum_{n=1}^{N} W(t_n)\, e^{-j2\pi f t_n} \qquad (1)$$

where the values of t_n with n running from 1 through N represent the time delays of the N taps.

SAW filters typically consist of a transmitter which generates surface waves and a set of receiving elements which tap the surface wave at various points along the propagation path. For a transmitter of width $\hat{L}$ and a receiver of width $\hat{\ell} = \rho\hat{L}$, separated by a distance $\hat{z}$ (hatted quantities are normalized to wavelengths) the signal at the receiver in response to unit voltage at the transmitter may be written as a function $R(\hat{L}, \rho\hat{L}, z)$.

If the receiving elements are connected to the bus bars through external attenuators then the received signal at any tap at a frequency f is written as,

$$U_R(f,t_n) = r(t_n)\cdot R(\hat{L},\rho(t_n)\cdot\hat{L},\hat{z}) \tag{2}$$

where $r(t_n)$ is the attenuation function.

In the absence of diffraction, the surface waves are plane and uniform across the aperture, so that,

$$\begin{aligned} R(\hat{L},\ \rho\hat{L},\ \hat{z}) &\propto \rho\cdot e^{-j2\pi\hat{z}} \\ &= \rho\cdot e^{-j2\pi ft} \end{aligned} \tag{3}$$

where, f = frequency and t = time delay.

The different methods for implementing a desired set of tap weights are broadly of two types:

(1) Varying overlap or apodized weighted transducers: Here the width of the receiving aperture is varied in accordance with the tap weight function, i.e., $\rho(t_n) = W(t_n)$ and $r(t_n) = 1$. The received signal is obtained from Eqs. (2) and (3) as,

$$\begin{aligned} U_R(f,t_n) = R[L,\ \rho(t_n)\cdot L,z] &\propto \rho(t_n)\cdot e^{-j2\pi ft_n} \\ &= W(t_n)\cdot e^{-j2\pi ft_n} \end{aligned} \tag{4a}$$

(2) Uniform overlap or unapodized weighted transducers: Here the receiving aperture is of constant width and the weighting is achieved by capacitive attenuators at each finger [3] or by selective withdrawal of fingers [4] or by series weighting [5]. We will discuss this class of devices with reference to the first method but it can be extended to the

other methods. In this method the tap attenuation function $r(t_n)$ is varied in accordance with the tap weight function, i.e., $r(t_n) = W(t_n)$ and $\rho(t_n) = 1$. The received signal is obtained from Eqs. (2) and (3) as,

$$U_R(f,t_n) = r(t_n)\cdot R(L,L,z) \propto r(t_n)\cdot e^{-j2\pi f t_n} = W(t_n)\cdot e^{-j2\pi f t_n} \tag{4b}$$

From Eqs. (4a) and (4b) we see that in the absence of diffraction both methods achieve the desired tap weighting as expressed by Eq. (1).

In the presence of diffraction $R(\hat{L}, \rho\hat{L}, \hat{z})$ is a more complicated function than expressed by Eq. (3). We will now discuss the theory of diffraction and apply it to determine this function.

2. Diffraction Theory

The theory of surface acoustic wave diffraction is basically an extension of the well-known principles of optical diffraction to anisotropic media and two dimensional wave propagation. Three different theoretical approaches have been described in the literature:

(1) Angular spectrum of plane waves [10,11]: This is a technique of Fourier analysis whereby a given source distribution is described in terms of its component plane waves with wave-vectors $\vec{K}$ in different directions. The wave amplitude of any field point is obtained by recombining the plane waves with appropriate phase-shifts. This technique thus involves an integration over K-space.

(2) Resolution into component Gaussian modes [12,13]: In this technique Gaussian waveforms are used as the basis rather than plane waves.

In isotropic space Gaussian beams represent 'normal modes' i.e., they retain their shape during propagation. This property remains valid in parabolic anisotropic space though not in general anisotropic space. This technique thus provides approximate analytical insights but is not suitable for numerical evaluation.

(3) Huygen's principle [9,15,17,19]: In this method the source is considered a collection of infinite point sources each of whose field distribution at a distance $\vec{R}$ is given by,

$$u = \frac{e^{j\vec{K}\cdot\vec{R}}}{\sqrt{R}}$$

The wave amplitude at any field point is obtained by summing the contributions from the individual point sources. This technique thus requires an integration over the source distribution.

Beam profile prediction on the basis of each of these approaches has been confirmed experimentally. However, the Huygen's function approach is most widely used because the integration over the source distribution is more well-defined and easier to perform numerically than the K-space integration required in the first method. Since the Huygen's function approach has been used in all our calculations, the other techniques will not be discussed further.

Application of Huygen's principle to parallel IDT transducers:

In this section the Huygen's principle will be applied to find the transfer function $R(\hat{L}, \rho\hat{L}, \hat{z})$ between a single finger transmitter and a single finger receiver as a function of their widths and separation.

This function may then be used to obtain the response of an actual filter which is made up of many such transmitter receiver pairs.

We will first take the special case when transmitter and receiver widths are equal. Consider (Figure 2) a single finger transmitter, T_X and a single finger receiver, R_X, each of width L separated by a distance Z. The problem is to find the amplitude and phase of the signal picked up by R_X relative to the transmitted signal.

In the Huygen's approach we assume T_X to be composed of a large number of point sources each of which has a contribution, u, at a distance $\vec{R}$ ($\vec{R}$ not too small) given by:

$$u \simeq \frac{e^{j\vec{K}\cdot\vec{R}}}{\sqrt{R}} \tag{5}$$

where $\vec{K}$ is the wave vector.

The signal at any point, X on the receiver is obtained by integrating u over the width of the transmitter:

$$U_X = \int_{\text{all } Y} u_{Y\to X}\, dy \tag{6}$$

The net signal at the receiver is obtained by integrating U_x over the receiver width:

$$R = \int_{\text{all } X} U_x\, dx = \int_{\text{all } X}\int_{\text{all } Y} u_{Y\to X}\, dxdy \tag{7}$$

For parallel line transmitting and receiving fingers (which is the most common case) the double integral in (7) is reducible to a single integral. This has been done by Szabo and Slobodnik [7] and by Mitchell and Stevens [6]. We derive this simplification in a slightly different

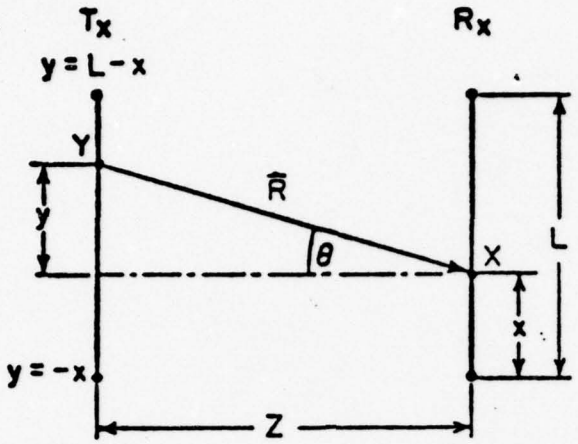

Figure 2. Parallel transmitter and receiver of equal width.

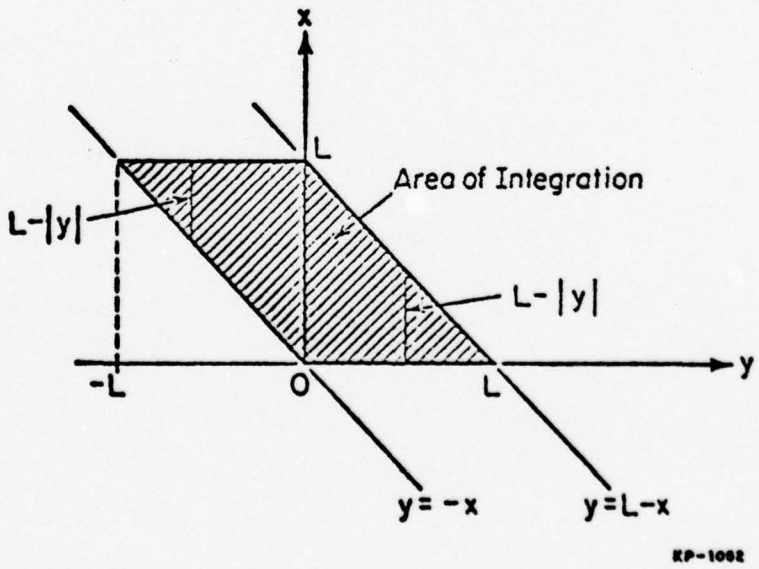

Figure 3. Area of integration for equal width transmitter and receiver.

manner to bring out the physical process involved in the reduction. The contribution at a point X on the receiver from a point Y on the transmitter is written as (Figure 2):

$$u_{Y\to X} = \frac{e^{jK\cdot r}}{\sqrt{r}} = \frac{e^{jK(\theta)\,\cdot\, Z\,\sec\,\theta}}{\sqrt{Z\,\sec\,\theta}} \tag{8a}$$

where θ is the angle made by the line YX with the axis (the Z-direction). Let x be the distance of the point X (on the receiver) as measured from the lower end of the receiver; and y be the distance of the pt. Y (on the transmitter) measured from the axial line (parallel to Z) through X, so that we have,

$$\tan\,\theta = \frac{y}{Z} \tag{8b}$$

With y thus defined, we see from Eq. (4a) that $u_{Y\to X}$ is a function of y and Z only and independent of x. We may write,

$$u_{Y\to X} = f(y,Z) \tag{8c}$$

With this definition of y and x, the signal at point X may be written as:

$$U_X = \int_{-x}^{L-x} dy\; f(y,Z)$$

The total receiver signal is given by:

$$R = \int_0^L dx \int_{-x}^{L-x} dy\; f(y,Z) \tag{9}$$

Equation (9) represents an integration in two coordinates, x and y. The area of integration on the y - x plane is shown in Figure 3. Since the integrand is a function of y alone, the x-integration may be eliminated

by multiplying the integrand by a factor L - $|y|$, equal to the x-dimension of the area of integration.

Thus, from Eq. (5),

$$R = \int_{-L}^{+L} dy\ (L - |y|)\ f(y,Z) \tag{10}$$

If $f(y,Z) = f(-y, Z)$ (which is true if $K(\theta) = K(-\theta)$), then,

$$R = 2 \int_{0}^{L} dy(Y - y)\ f(y,Z) \tag{11}$$

The result of Eq. (10) may be visualized physically as follows: The double integral in (7) basically means that we have to sum the contributions of all of the rays that are drawn from each point on the transmitter to each point on the receiver.

Consider (Figure 4) the ray from one end of the transmitter C to a point, X on the receiver such that the distance of C above the axial line through X is y_1. Then,

$$u_{C\to X} = f(y_1, Z)$$

Now, for each point, M on the receiver between X and B (the lower end) we find a point N on the transmitter such that NM is parallel to CX. Since parallel rays are equivalent,

$$u_{N\to M} = u_{C\to X} = f(y_1, Z)$$

However, paralliel rays like PQ at points, P outside BX do not end on the transmitter and hence do not contribute to our integral. Thus a particular contribution $f(y_1, Z)$ will be weighted by a factor proportional to the length of BX(= $L-y_1$) in our summation process. So,

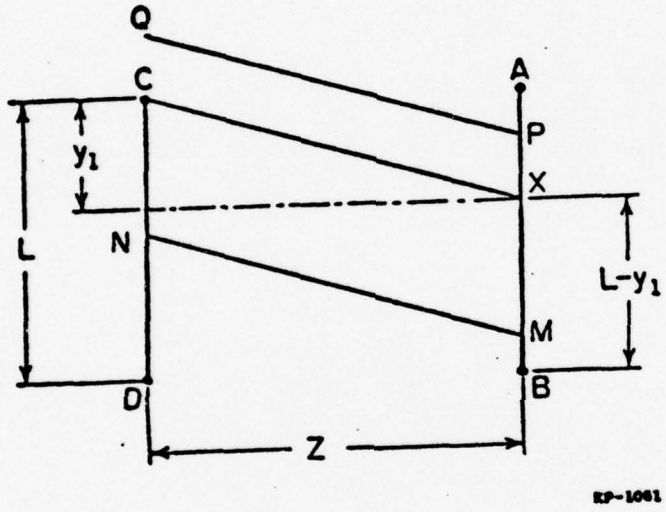

Figure 4. Parallel transmitter and receiver of equal width.

$$R = \sum_{\text{all } y_1} (L - |y_1|)\, f(y_1, Z)$$

$$= \int_{-L}^{+L} dy\, (L - |y|)\, f(y, Z)$$

A similar reasoning may be applied with unequal transmitter and receiver width (Figure 5). From the area of integration (Figure 6) it follows that in this general case,

$$R = \int_{a}^{b} dx \int_{-x}^{L-x} dy\, f(y, Z)$$

$$= \int_{-b}^{-a} dy(b + y)\, f(y, Z) + \int_{-a}^{L-b} dy(b - a)\, f(y, Z)$$

$$+ \int_{L-b}^{L-a} dy(L - y - a)\, f(y, Z) \qquad (12)$$

If the receiver is symmetrically located with respect to the transmitter (which is usually the case in apodized transducers), we have, $L - b = a$, $L - a = b$, so that from (12),

$$R = \int_{-b}^{-a} dy(b - |y|)\, f(y, Z) + \int_{-a}^{a} dy(b - a)\, f(y, Z)$$

$$+ \int_{a}^{b} dy(b - y)\, f(y, Z)$$

$$= 2\left[\int_{0}^{a} dy(b - a)\, f(y, Z) + \int_{a}^{b} dy(b - y)\, f(y, Z) \right]$$

if $\quad k(\theta) = k(-\theta).$ $\qquad (13)$

The transfer function has been derived above without any approximations and so may be used for any kind of anisotropy provided the function $k(\theta)$ is known accurately.

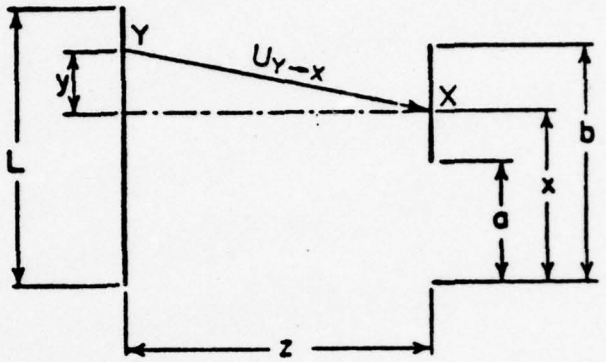

Figure 5. Parallel transmitter and receiver of unequal width.

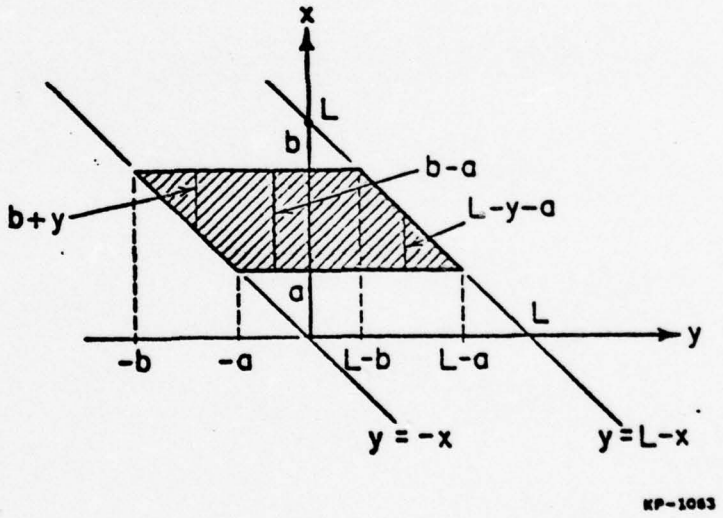

Figure 6. Area of integration for unequal width transmitter and receiver.

3. Fresnel's Approximation

In many practical cases $k(\theta)$ is approximated by a parabolic function of the form,

$$k(\theta) \simeq k_o\left(1 - \frac{\gamma}{2}\theta^2\right)$$

where k_o is the wavevector in the z-direction (Figure 1) and γ is a parameter depending on the particular crystal and axis of propagation.

In parabolically anisotropic space beam diffraction is the same as in isotropic space with the distance scaled by a factor $(1 + \gamma)$ [9,10,12] i.e., the effective distance $\hat{z}_{eff}$ is given by

$$\hat{z}_{eff} = \hat{z}(1 + \gamma)$$

In this case the Fresnel's approximation can be used when $\hat{z}_{eff} > \hat{L}$ (hatted quantities are referred to wavelengths). Under this approximation the integrals in Eq. (13) reduce to the Fresnel's integral. Since this integral is available in tabulated form, a considerable reduction in computation time is achieved by the approximation.

Using the Fresnel's approximation the transfer function between a transmitter and receiver of equal width $\hat{L}$ and separation $\hat{z}$ is written as:

$$R(\hat{L},\hat{L},\hat{z}) = e^{-j2\pi\hat{z}}\sqrt{\hat{z}(1+\gamma)}\left[\frac{\hat{L}}{\sqrt{\hat{z}/2(1+\gamma)}}\int_0^{L/\sqrt{\hat{z}/2(1+\gamma)}} dv\, e^{-j\pi v^2/2} - \frac{j}{\pi}\left\{\exp\left(-\frac{j\pi}{2}\,\frac{\hat{L}^2}{\hat{z}/2(1+\gamma)}\right) - 1\right\}\right] \tag{14}$$

The transfer function R does not depend separately on $\hat{z}$ and $\hat{L}$ but on $\hat{L}^2/\hat{z}(1+\gamma)$. Utilizing this fact R is written as,

$$R(\hat{L},\hat{L},\hat{z}) = e^{-j2\pi\hat{z}} \cdot \sqrt{2}\ \hat{L}\cdot S(F) \tag{15}$$

where $$S(F) = \mathcal{F}r\sqrt{\frac{2F}{\pi}} - \frac{j}{\sqrt{2F\pi}}\ (e^{-jF} - 1)$$

$$F = \pi\hat{L}^2/\hat{z}(1+\gamma)$$

and $\mathcal{F}r\ x$ is the Fresnel's integral $\int_0^x dv\ e^{-j\pi v^2/2}$.

Similarly for a transmitter of width $\hat{L}$ and receiver of width $\rho\hat{L}$ ($\rho < 1$) separated by a distance $\hat{z}$, the transfer function (Eq. (13)) is written as:

$$R(\hat{L},\ \rho\hat{L},\ \hat{z}) = e^{-j2\pi\hat{z}} \cdot \sqrt{\hat{z}(1+\gamma)}$$

$$\left[\frac{\hat{b}}{\sqrt{\hat{z}/2(1+\gamma)}}\int_0^{\hat{b}/\sqrt{\hat{z}/2(1+\gamma)}} dv\ e^{-j\pi v^2/2} - \frac{\hat{a}}{\sqrt{\hat{z}/2(1+\gamma)}}\int_0^{\hat{a}/\sqrt{\hat{z}/2(1+\gamma)}} dv\ e^{-j\pi v^2/2}\right.$$

$$\left. - \frac{j}{\pi}\left\{\exp\left(-\frac{j\pi}{2}\,\frac{\hat{b}^2}{\frac{\hat{z}}{2}(1+\gamma)}\right) - \exp\left(-\frac{j\pi}{2}\,\frac{\hat{a}^2}{\hat{z}/2(1+\gamma)}\right)\right\}\right] \tag{16}$$

where $\rho\hat{L} = \hat{b} - \hat{a}$ (Figure 4). If the receiver is symmetrically located, then,

$$\hat{b} = \hat{L}\,\frac{1+\rho}{2}$$

$$\hat{a} = \hat{L}\,\frac{1-\rho}{2}$$

Comparing with Eq. (11), Eq. (12) is written as,

$$R(\hat{L},\ \rho\hat{L},\ \hat{z}) = R(\hat{b},\hat{b},\hat{z}) - R(\hat{a},\hat{a},\hat{z})$$

$$= e^{-j2\pi\hat{z}} \cdot \sqrt{2}\ \hat{L} \cdot \left[\frac{1+\rho}{2}\,S(F_b) - \frac{1-\rho}{2}\,S(F_a)\right] \tag{17a}$$

where $$F_b = \frac{\pi \hat{b}^2}{\hat{z}(1+\gamma)} = F\left(\frac{1+\rho}{2}\right)^2 \tag{17b}$$

$$F_a = \frac{\pi \hat{a}^2}{\hat{z}(1+\gamma)} = F\left(\frac{1-\rho}{2}\right)^2$$

Thus, $$R(\hat{L}, \rho\hat{L}, \hat{z}) = e^{-j2\pi\hat{z}\sqrt{2}\cdot\hat{L}} S(F,\rho) \tag{18a}$$

where $$S(F,\rho) = \frac{1+\rho}{2} S(F_b) - \frac{1-\rho}{2} S(F_a) \tag{18b}$$

We now have the transfer function between two parallel fingers in a form suitable for evaluating the response of unapodized (Eq. (15)) and apodized (Eq. (18)) devices.

4. Nature of Diffraction Errors in Apodized and Unapodized Devices

A function $E(F,\rho)$ is defined,

$$E(F,\rho) = R(\hat{L}, \rho\hat{L}, \hat{z})/\rho e^{-j2\pi\hat{z}}$$

that compares the transfer function R with diffraction (Eq. (18)) to its no diffraction value of $\rho e^{-j2\pi\hat{z}}$ (Eq. (3)). The actual tap weights, W_D with diffraction are given by,

$$W_D = W \cdot E(F,\rho)$$

where W represent the ideal tap weight without diffraction.

Figures 7 and 8 show the amplitude and phase of E for different values of ρ as a function of the normalized aperture separation factor, ASF which is related to F by

$$ASF = \pi/F = \hat{z}(1+\gamma)/L^2$$

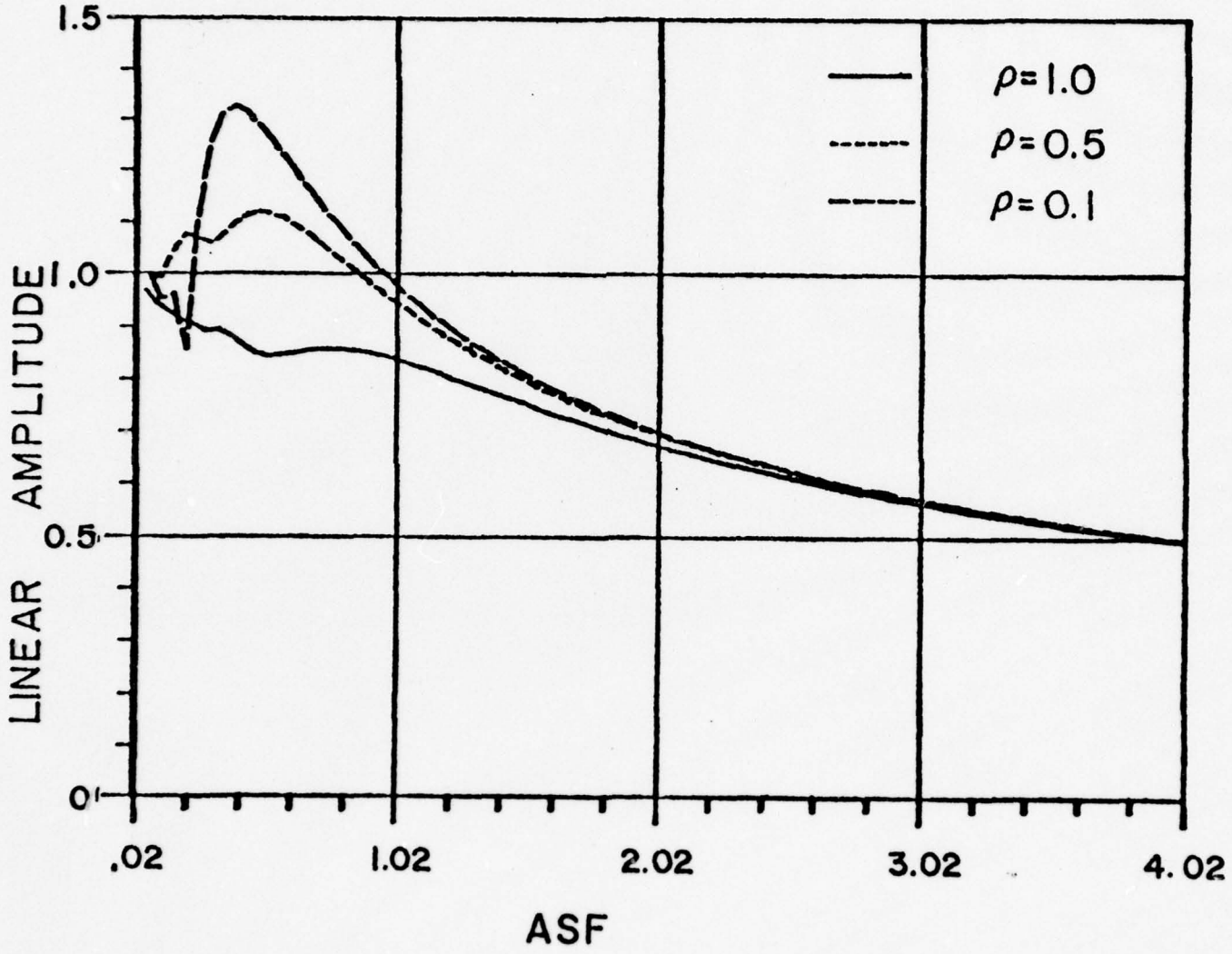

Figure 7. Amplitude (normalized with respect to no-diffraction value) of received signal as a function of aperture separation factor for different ratios of receiver and transmitter widths.

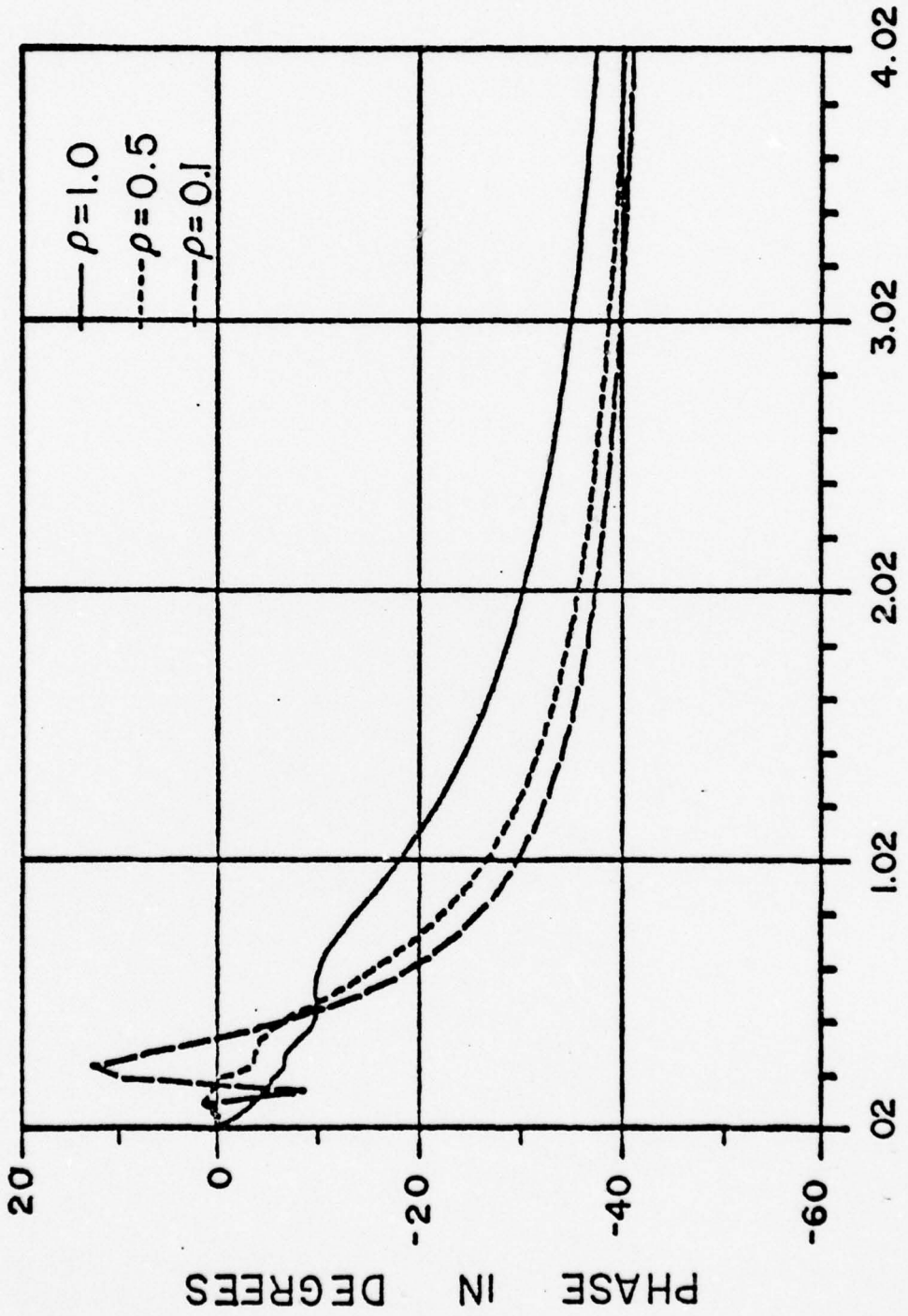

Figure 8. Phase of received signal as a function of aperture separation factor for different ratios of receiver and transmitter widths.

Tap errors are incurred because of changes in E from one tap to another. The change in E from one tap to the next is written approximately as,

$$\Delta E \simeq \frac{\partial E}{\partial \hat{z}} \cdot \Delta z + \frac{\partial E}{\partial \rho} \cdot \Delta \rho$$

$$= \frac{\partial E}{\partial (ASF)} \cdot \frac{\partial (ASF)}{\partial \hat{z}} \Delta z + \frac{\partial E}{\partial \rho} \cdot \Delta \rho$$

$$= \frac{\partial E}{\partial (ASF)} : \frac{1+\gamma}{\hat{L}^2} \cdot \Delta \hat{z} + \frac{\partial E}{\partial \rho} \cdot \Delta \rho \qquad (19)$$

where $\Delta \hat{z}$ is the change in $\hat{z}$ and $\Delta \rho$ is the change in ρ from one tap to the next.

It is seen from Figures 7 and 8 that for ASF > 1 the function E becomes relatively smooth. This is the far field region where diffraction errors are less because of the lower values of the derivatives in Eq. (19a). However, practical devices cannot be built in the far field because there is a large waste of power and substrate area.

In the near field (ASF < .05) the diffraction errors are low. However, because of the limited extent of this region and RF coupling problems devices cannot be located totally in the near field. In the intermediate field (where most devices are built) the errors are larger. However, for unapodized devices the second term in Eq. (19a) is absent (ρ = 1 for all taps) and the first term may be made sufficiently small by increasing $\hat{L}$ as discussed by Wagers [8]. In practice $\hat{L}$ cannot be increased indefinitely because of limited substrate size and correction techniques are called for.

Since apodized devices have a wide variation of ρ for different taps, diffraction errors are considerably larger due to the second term in Eq. (19a) and cannot be removed by mere increase of $\hat{L}$. A typical apodized filter has diffraction errors ~30db below passband level as compared to ~50 db for unapodized filters.

5. Frequency-Dependent and Frequency-Independent Tap Models for Diffraction

In analogy with Eqs. (2), (3), and (4), the transfer function R is written as (from Eq. (18)),

$$U_R(f,t_n) = r(t_n)\cdot R(\hat{L},\ \rho(t_n)\cdot\hat{L},\ \hat{z}) = e^{-j2\pi\hat{z}}\cdot W_D(f,t_n)$$

where $$W_D = \sqrt{2}\ L\ S(F,\rho)\cdot r(t_n)$$

f = frequency

W_D represents the actual frequency dependent complex tap-weight including the effects of diffraction. The frequency dependence arises because F varies with frequency. The distorted frequency response due to diffraction is given by

$$H_D(f) = \sum_{n=1}^{N} W_D(f,t_n)\ e^{-j2\pi f t_n} \qquad (20)$$

Equation (20) is used in conjunction with Eq. (18) to evaluate the response of an actual device. We will call this the frequency dependent tap model (FDT) since it takes into account the frequency dependence of individual tap response due to diffraction. Device response predictions on the basis of this model have been experimentally verified by Mitchell and Stevens [6]

and by Szabo and Slobodnik [7]. This method, though quite accurate, has the disadvantage of requiring a large amount of computation time.

A considerable reduction in computation time is achieved if the frequency dependence of W_D is neglected, i.e., if $W_D(f,t_n)$ is replaced by its value at some convenient frequency, f_0, possibly the center frequency. For typical narrowband filters this is a very good approximation. With this approximation, Eq. (19) becomes,

$$H_D(f) \simeq \sum_{n=1}^{N} W_D(f_0,t_n)\, e^{-j2\pi f t_n} \tag{21}$$

We will call this the frequency independent tap (FIT) model. Computationally it is far faster than the FDT because.

(1) W_D needs only to be calculated for one frequency instead of each frequency of interest and

(2) The efficient fast Fourier transform may be used in computing $H_D(f)$.

For a typical narrowband filter it takes only a few seconds for the FIT model compared to a few minutes for the FDT model.

The FIT model is particularly significant because it represents the limit to which diffraction errors may be corrected during filter design. The process of correction involves determining the right overlap functions and delays $\rho(t_n)$ for apodized devices (or the right attenuation function and delay $r(t_n)$ for unapodized devices) so that the diffracted tap weights $W_D(f,t_n)$ accurately reproduce the desired tap weight function $W(t_n)$. However, this can only be done for a single frequency, f_0, such that

$W_D(f_0,t_n) = W(t_n)$. No technique is known to tailor the amplitude and delay of a single tap so as to compensate for the frequency variation of diffraction effects. The added accuracy of the FDT model is thus only of analytical value; it cannot be used to improve performance. The accuracy of which the FIT model reproduces the FDT model represents the ultimate accuracy to which diffraction corrections may be effected.

In Chapter II we will describe in detail the accuracy of the FIT model in various cases and how the accuracy may be improved for unapodized devices by a judicious choice of f_0. For the present it suffices to mention that for narrowband apodized devices without diffraction correction the predictions from the two models agree very closely. The experimental results presented in this chapter relate to apodized devices that fall into this category.

6. Experimental Results

Experimental results with apodized devices for ST cut quartz ($\gamma = .378$) are presented in this section. The first filter has a 400-tap output transducer and a short input transducer. The maximum transducer width is 50 wavelengths and the center to center distance is 190 wavelengths.

Figure 9a shows the response predicted with diffraction from the FIT and FDT models. The two agree quite well. Figures 9b and 9c show the experimental response together with the theoretical response with and without diffraction. Evidently, the sidelobes near the edge of the passband are predicted quite well by the theory.

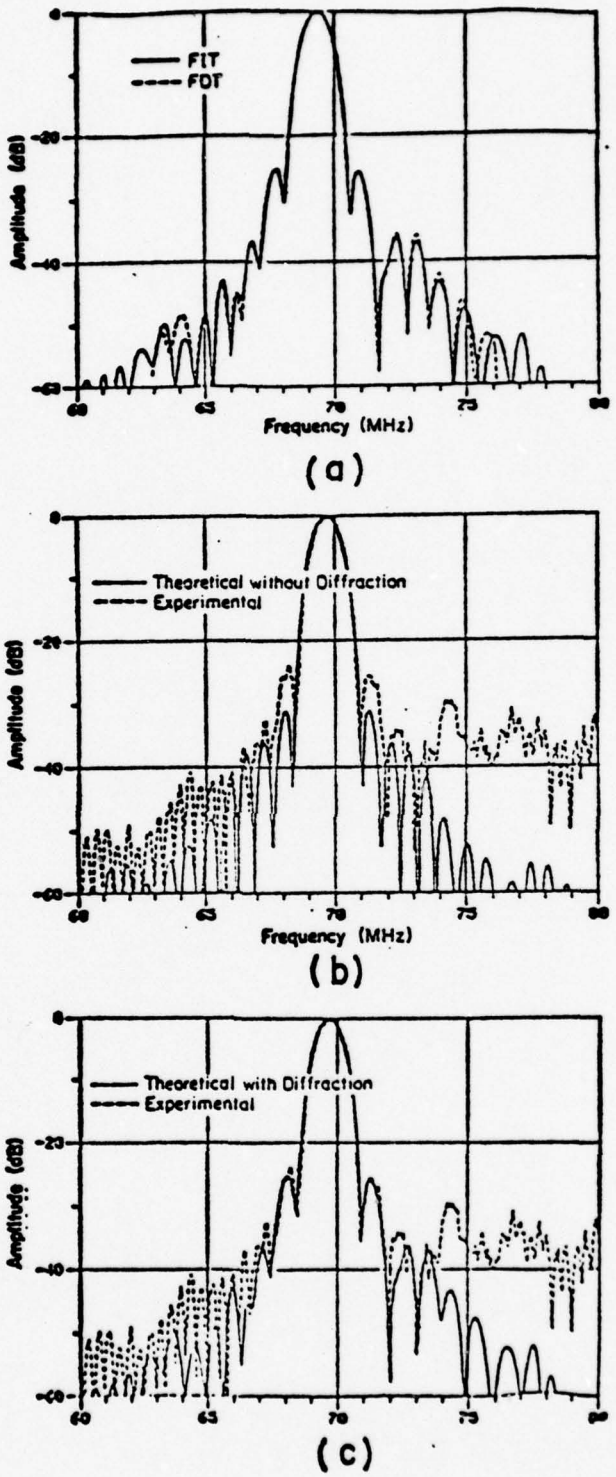

Figure 9. Predicted and experimental response for apodized filter.
(a) Predicted response with diffraction from FIT and FDT models.
(b) Predicted response without diffraction and experimental response.
(c) Predicted response with diffraction and experimental response.

Figure 10a shows the theoretical response with and without diffraction for another filter with a short input transducer and 351-tap apodized output transducer. Figure 10b shows the experimental response and the predicted response (with diffraction). On the low side the lobes are predicted convincingly. Lack of agreement on the high side is because of the presence of bulk waves due to the wider bandwidth of this filter. This is evident from Figure 11 which shows the bulk wave response obtained by absorbing out the surface waves.

7. Concluding Remarks

In this chapter an analysis of diffraction suitable for application to surface wave devices has been described. The simplification obtained by assuming an FIT model is discussed. A full discussion of the approximations involved in this model will be presented in the following chapter. Experimental results for two filters is presented in confirmation of the analysis procedure. The analysis has not been verified for capacitive weighted devices since this technique has as yet been used only on $LiNbO_3$ which has a non-parabolic velocity surface.

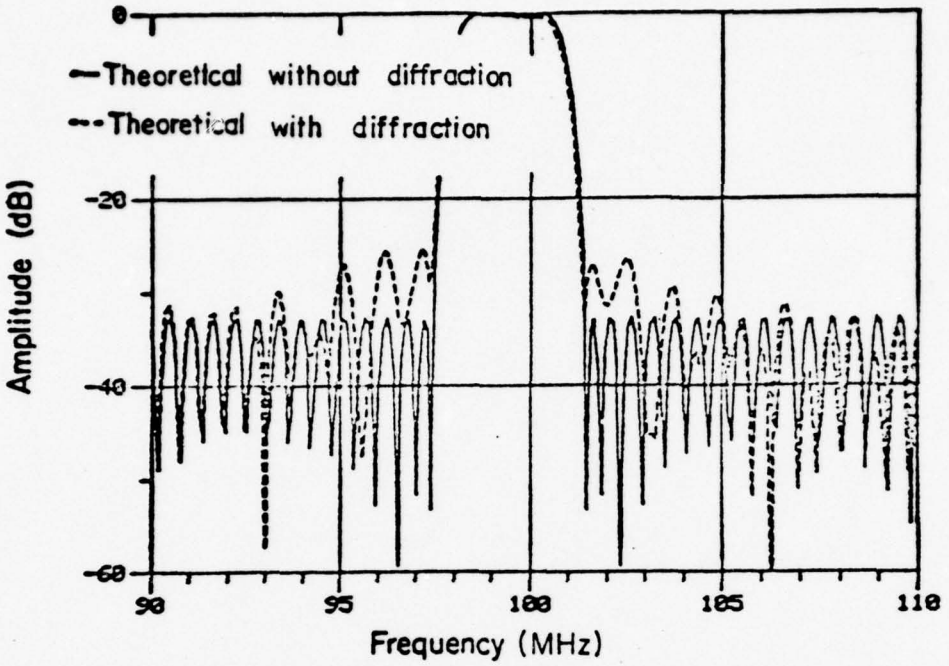

(a)

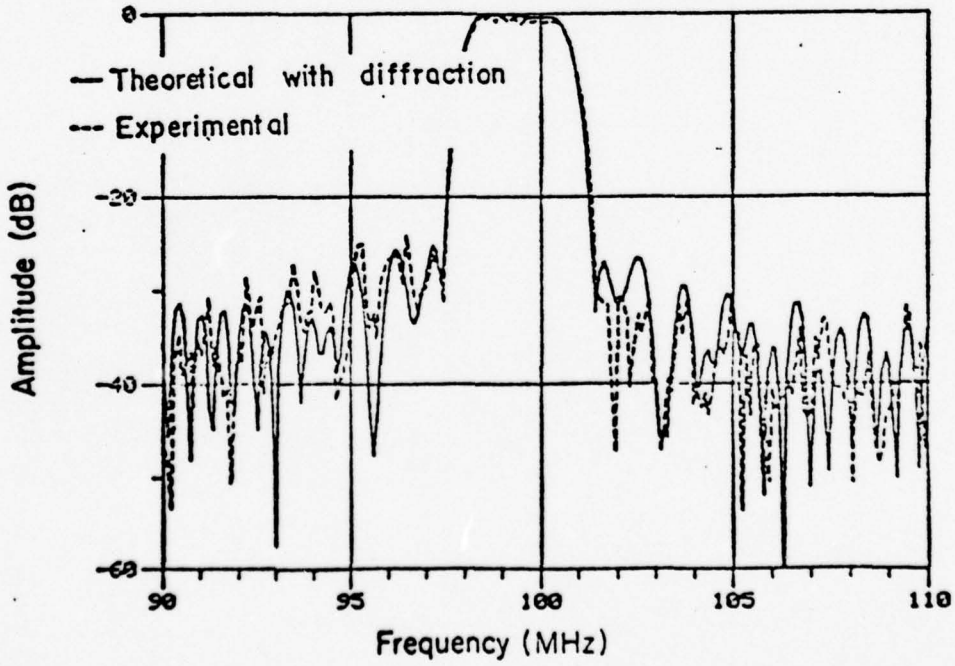

(b)

Figure 10. Predicted and experimental response for a second apodized filter.
(a) Predicted response with and without diffraction
(b) Predicted response with diffraction and experimental response

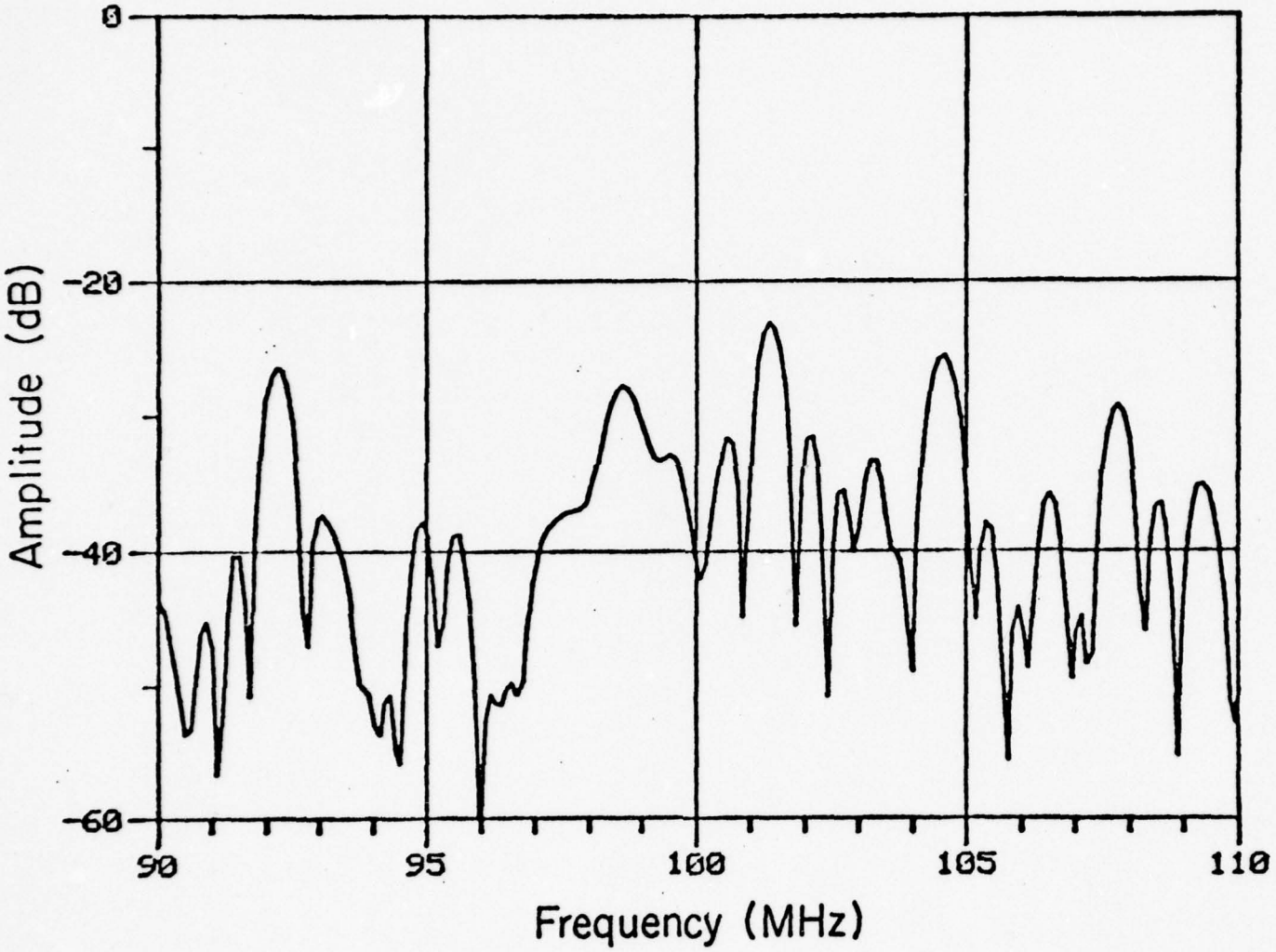

Figure 11. Experimental bulk wave response obtained by absorbing out surface waves.

CHAPTER II - DIFFRACTION-COMPENSATED DESIGN

This chapter discusses the design of SAW filters with optimum diffraction compensation pointing out the limitations imposed by the frequency dependence of diffraction errors. Possible techniques for effecting tap weight and delay corrections are described. A practical implementation of the correction procedure is presented.

1. Limits to Diffraction Correction

The impulse response model [1], which is widely used in the analysis and design of SAW filters, assumes a constant strength and linear phase response with frequency for individual taps. In the presence of diffraction this assumption is violated; and accurate diffraction analysis calls for a frequency dependent tap (FDT) model that takes into account the frequency variations in individual tap response.

The FDT model cannot, however, be used in correcting diffraction errors since the diffraction-induced variations in individual tap response with frequency cannot be compensated by any known technique. Earlier works directed at compensating for diffraction errors during device design [7,8,18] have all carried out diffraction calculations at center frequency, thus using a frequency independent tap (FIT) model (or the impulse response model) for correction - a model that neglects the frequency dependence of the response of individual taps.

The difference between the FIT and the FDT models represents an error that established a fundamental limit on the optimum performance that can possible be achieved in the presence of diffraction. The extent of this limit for apodized and unapodized filters are discussed in this section.

All examples quoted in this section are for single filters with only one transducer weighted, the other being of short time extent. The maximum width of the transducers is assumed to be 50 wavelengths. The distance of the input transducer to the near end of the output transducer is assumed 90 wavelengths; so that the devices are located in the near and intermediate fields. The substrate material is assumed to be ST quartz with an anisotropy scaling factor of $\gamma = 0.378$ [9].

(a) Unapodized Devices

For unapodized transducers with the receiving elements connected to the bus bars through external attenuators, the received signal at any element is written as (from Eq. (2)),

$$U_R(f,t_n) = r(t_n)\cdot R(\hat{L},\hat{L},\hat{z}) \tag{22}$$

The function $R(\hat{L},\hat{L},\hat{z})$ has been derived in Eq. (15) as

$$R(\hat{L},\hat{L},\hat{z}) = e^{-j2\pi\hat{z}}\sqrt{2}\,\hat{L}\cdot S(F) \tag{15}$$

where

$$S(F) = FR\sqrt{\frac{2F}{\pi}} - \frac{j}{\sqrt{2F\pi}}\,(e^{-jF}-1)$$

$$F = \frac{\pi\hat{L}^2}{\hat{z}(1+\gamma)} = \frac{\pi(L/\lambda)^2}{z/\lambda(1+\gamma)}$$

(λ = wavelength).

The parameter F varies directly with frequency and is written as,

$$F = F_0 \cdot \frac{f}{f_0} \tag{22a}$$

where the subscript 0 indicates the value at $f = f_0$. Similarly,

$$\hat{L} = L_0 \cdot \frac{f}{f_0} \tag{22b}$$

Equations (22) and (15) are combined to yield,

$$U_R(f,t_n) = r(t_n) \cdot e^{-j2\pi\hat{z}} \cdot \sqrt{2}\, \hat{L} \cdot S(F)$$

$$= e^{-j2\pi f t_n} \cdot r(t_n) \cdot \sqrt{2}\, \hat{L} \cdot S(F) \tag{23}$$

Comparing Eqs. (23) and (4a) we write the tap weight including the effects of diffraction as,

$$W_D(f,t_n) = r(t_n) \cdot \sqrt{2}\, \hat{L} \cdot S(F) \tag{24a}$$

At $f = f_0$,

$$W_D(f_0,t_n) = r(t_n) \cdot \sqrt{2}\, L_0 \cdot S(F_0) \tag{24b}$$

Using Eqs. (22a) and (22b), Eq. (24a) is expanded around $f = f_0$ for small changes Δf in frequency from f_0,

$$W_D(f,t_n) = r(t_n) \cdot \sqrt{2} \cdot L_0 \cdot \left[S(F_0) + \frac{\Delta f}{f_0} (S(F_0) + D(F_0))\right]$$

where $$D(F_0) = F_0 \frac{dS(F_0)}{dF_0} = j(e^{-jF_0} - 1) \sqrt{\frac{1}{8F_0\pi}}$$

For a given value of L_0, $S(F_0)$ and $D(F_0)$ may be written as $S(t)$ and $D(t)$ respectively, since F_0 is given by,

$$F_0 = \frac{\pi L_0^2}{z(1+\gamma)} = \frac{\pi L_0^2}{f_0 - t(1+\gamma)}$$

Thus, dropping the constant multiplier $\sqrt{2}\cdot L_0$,

$$W_D(f,t_n) = r(t_n)[S(t_n) + \frac{\Delta f}{f_0}\{S(t_n) + D(t_n)\}] \tag{25a}$$

$$= W_D(f_0,t_n) + \frac{\Delta f}{f_0}\cdot r(t_n)\cdot(S(t_n) + D(t_n)) \tag{25b}$$

and $$W_D(f_0,t_n) = r(t_n)\cdot S(t_n) \tag{25c}$$

The second term in Eq. (25b) represents the tap weight error incurred in the FIT model.

To determine the effect of this error on the frequency response we use Eq. (20),

$$H_D(f) = \sum_{n=1}^{N} W_D(f,t_n)\, e^{-j2\pi f t_n}$$

$$= \sum_{n=1}^{N} e^{-j2\pi f t_n}\, r(t_n)[S(t_n) + \frac{\Delta f}{f_0}\{S(t_n) + D(t_n)\}]$$

For an uncorrected device, the attenuation function is the same as the tap weight function.

$$r(t_n) = W(t_n)$$

and the specified frequency response is given by (Eq. (1)),

$$H(f) = \sum_{n=1}^{N} W(t_n)\cdot e^{-j2\pi f t_n}$$

$$\therefore H_D(f) = H(f)*S(f) + \frac{\Delta f}{f_0}\cdot[H(f)*(S(f) + D(f))] \tag{26a}$$

where $$S(f) = \sum_{n=1}^{N} S(t_n)\, e^{-j2\pi f t_n}$$

$$D(f) = \sum_{n=1}^{N} D(t_n)\, e^{-j2\pi f t_n}$$ and * denotes convolution.

The diffracted response predicted by the FIT model is obtained as,

$$H_D^0(f) = \sum_{n=1}^{N} W_D(f_0, t_n) \cdot e^{-j2\pi f t_n}$$

$$= \sum_{n=1}^{N} r(t_n) \cdot S(t_n) \cdot e^{-j2\pi f t_n}$$

$$= H(f) * S(f) \qquad (26b)$$

The difference between the two models is then given by [Eqs. (26a) and (26b)],

$$\frac{\Delta f}{f_0} \cdot \{H(f) * (S(f) + D(f))\} \qquad (26c)$$

The difference becomes appreciable when

$$S(f) \simeq \frac{\Delta f}{f_0} \cdot (S(f) + D(f)) \ .$$

Figure 12 shows $S(f)$ and $S(f) + D(f)$ for the special case of $L_0 = 40$ and $\gamma = 0$. ($S(f)$ and $S(f) + D(f)$ are actually centered around 0 MHz but have been plotted around 100 MHz in the figure for ease of reference). Since the latter is an order of magnitude larger than the former we may expect that even for moderate values of $\Delta f/f_0$ the error in the FIT model may be appreciable. Figure 13a and 13b show the predicted frequency response from the FDT and FIT models for 1% and 2% bandwidth filters respectively.

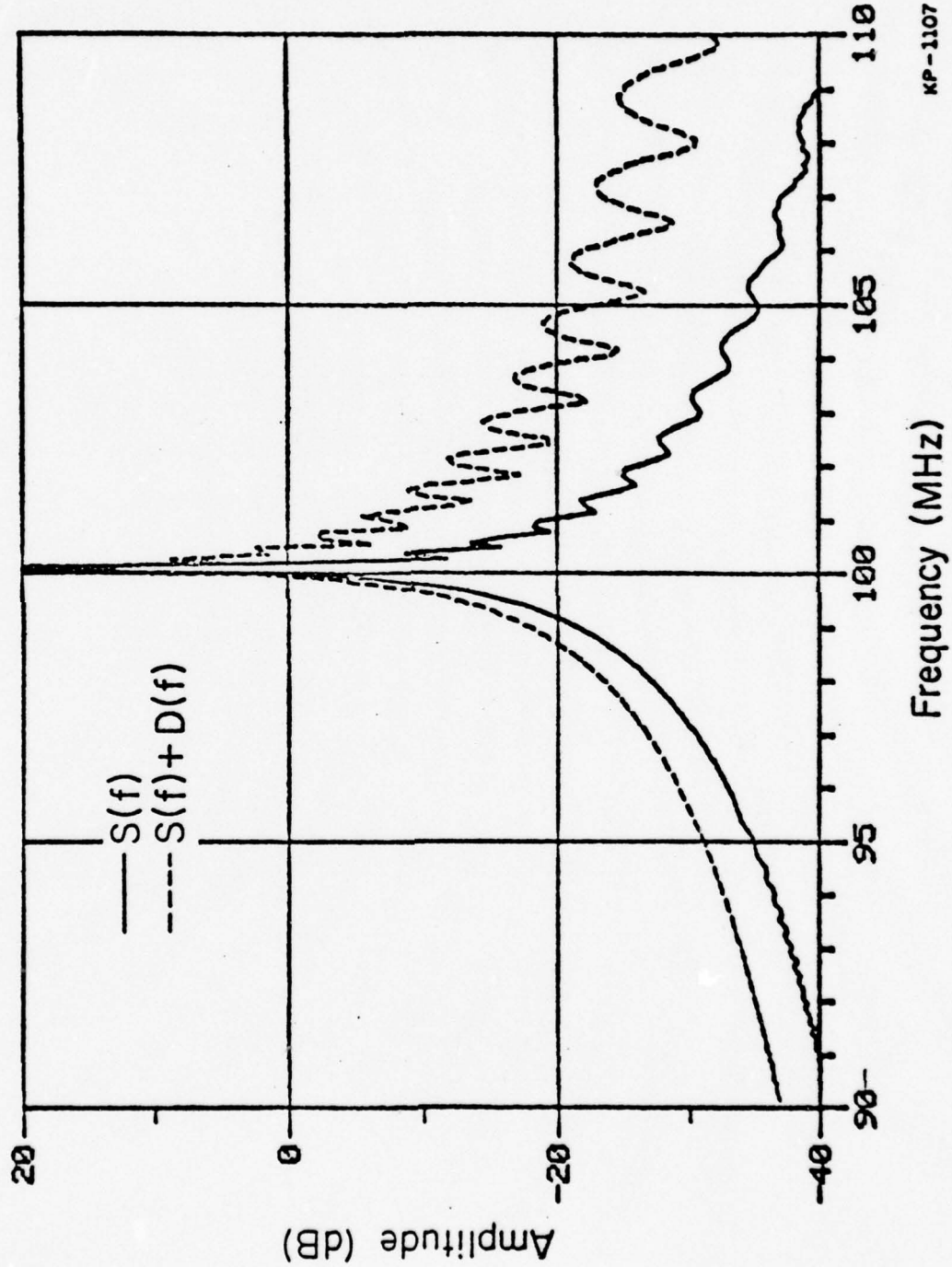

Figure 12. Comparing S(f) with S(f) + D(f).

For $\Delta f/f_0 = .01$ (Figure 13a) the difference is negligible, but for $\Delta f/f_0 = .02$ (Figure 13b) there is a small difference.

These small differences, however, become important when the devices are corrected.. Correction involves the determination of an attenuation function $r(t_n)$ that yields the desired tap weight function with diffraction at some specified $f = f_0$, i.e., $W_D(f_0,t_n) = W(t_n)$. Clearly from Eq. (25c), $r(t_n) = W(t_n)/S(t_n)$ such that, from Eq. (25b), the tap weight with diffraction are given by

$$W_D(f,t_n) = W(t_n) + \frac{\Delta f}{f_0} \cdot W(t_n) \cdot \frac{S(t_n) + D(t_n)}{S(t_n)} \tag{27a}$$

Thus, for a device with the best possible diffraction correction (assuming complete accuracy in the adjustment of tap weights and delays and negligible errors from other sources),

$$H_D(f) = \sum_{n=1}^{N} W_D(f,t_n)\, e^{-j2\pi f t_n}$$

$$= H(f) + \frac{\Delta f}{f_0} H(f) * C(f) \tag{27b}$$

where

$$C(f) = \sum_{n=1}^{N} \frac{S(t_n) + D(t_n)}{S(t_n)}\, e^{-j2\pi f t_n} \tag{27c}$$

The term $\Delta f/f_0 \cdot H(f) * C(f))$ in Eq. (27b) thus represents a diffraction error that may not be corrected away. Figures 14a and 14b show the predicted response from the FDT and FIT models for the corrected filters with f_0 at center frequency (100 MHz). For the filter with 2% bandwidth we see that nothing is gained from the correction (Figure 14b). For the filter with 1% bandwidth there is some gain but not as much as expected from the FIT model (Figure 14a).

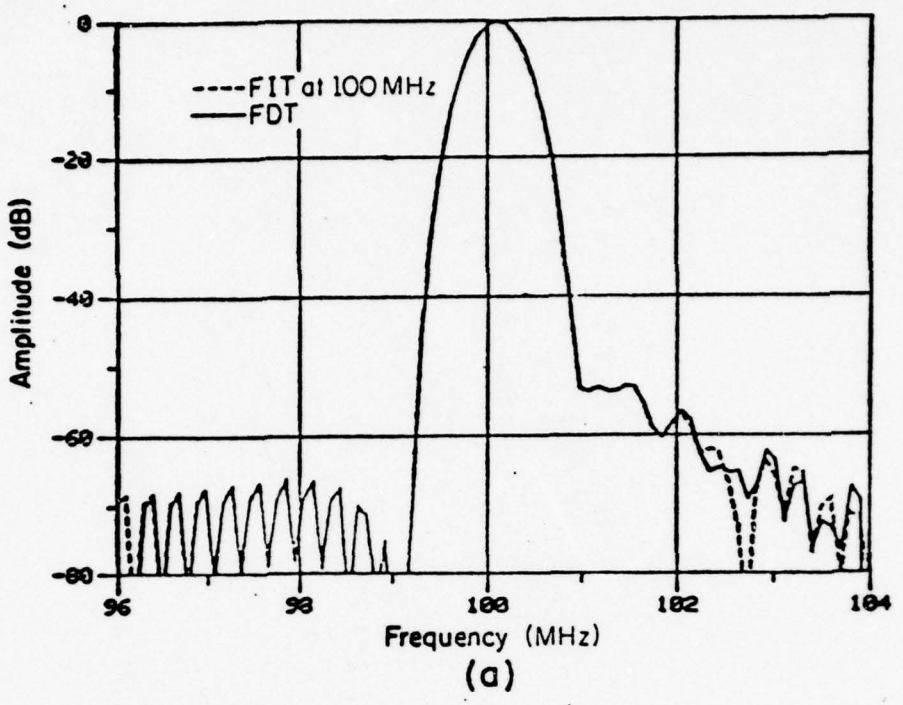

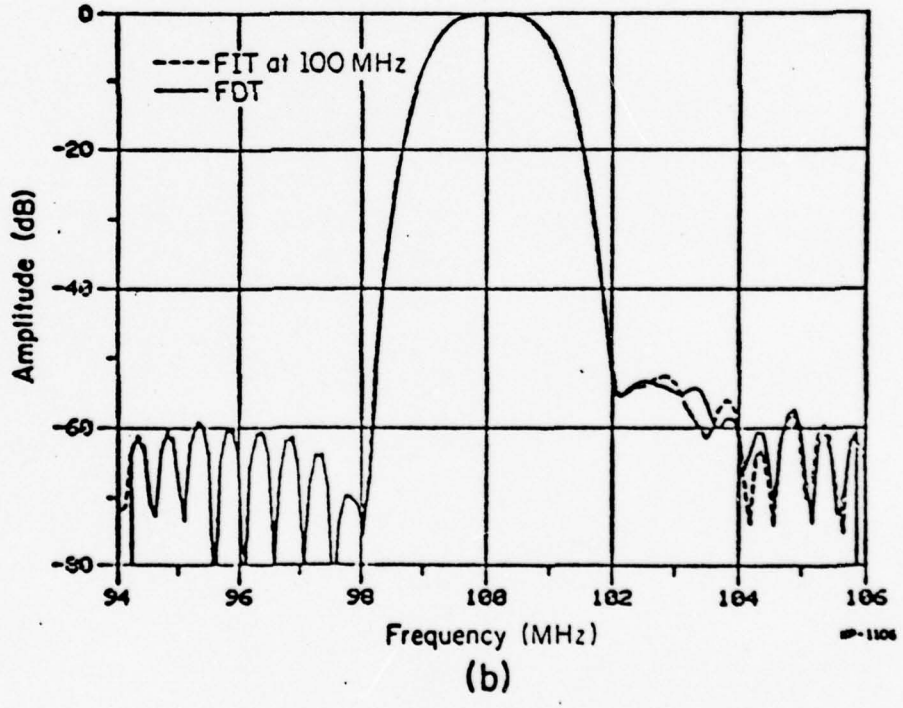

Figure 13. Response with diffraction calculated from the FDT model and the FIT model (at center frequency) for unapodized
(a) 1% bandwidth filter.
(b) 2% bandwidth filter.

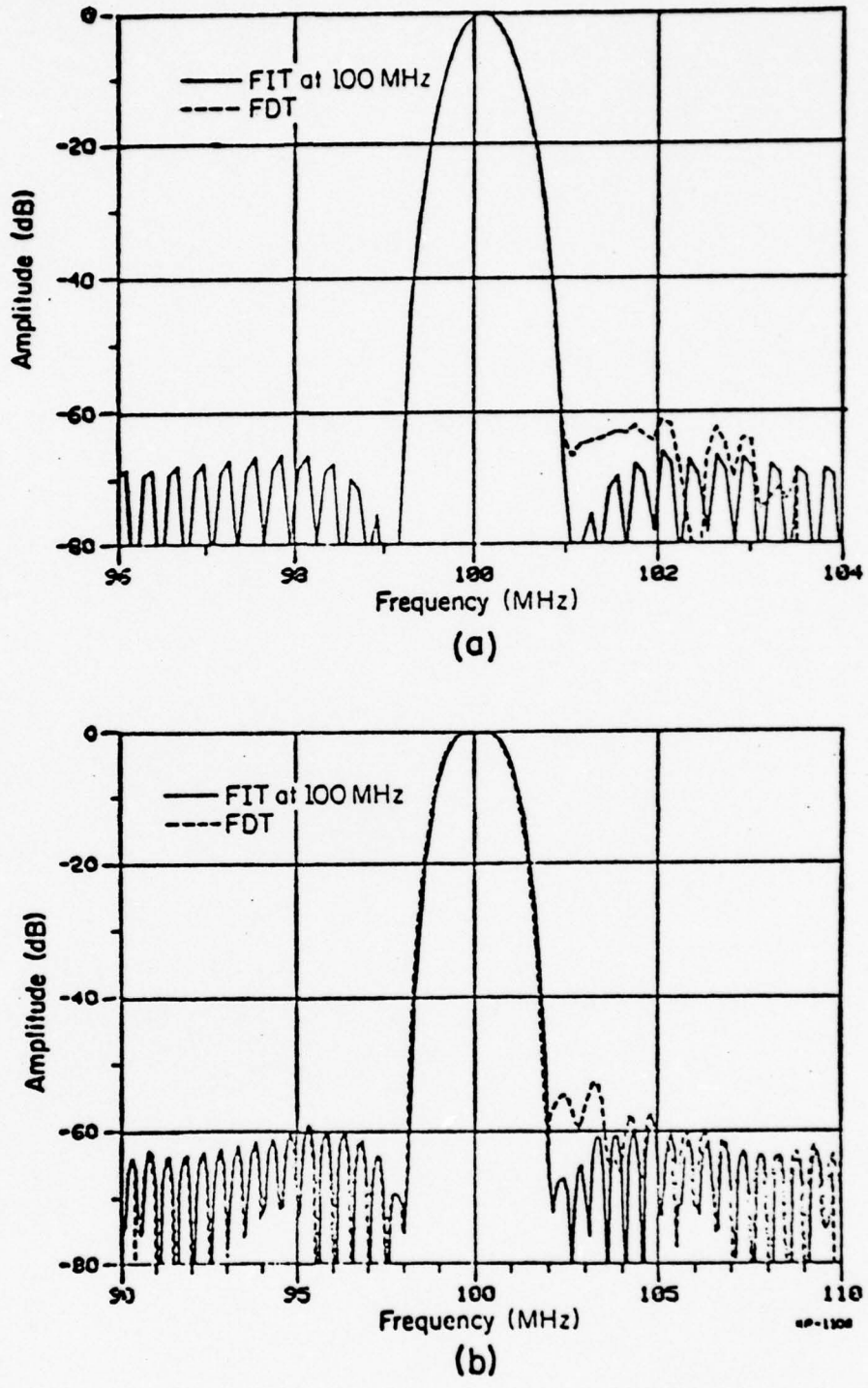

Figure 14. Response with diffraction calculated from the FDT model and the FIT model (at center frequency) for unapodized
(a) 1% bandwidth filter corrected at 100 MHz.
(b) 2% bandwidth filter corrected at 100 MHz.

However, because the errors are localized in the upper transition region of the frequency function, the error may be minimized by choosing f_0 not at center frequency but at a higher frequency in the region of distortion. This makes $\Delta f = 0$ right around the frequencies of maximum error (Eq. (27b)).

Figure 15b shows the predicted responses from the FDT and FIT models for the 2% bandwidth filter corrected at 103.5 MHz in place of 100 MHz. The correction is near perfect. Figure 15a shows the same for the 1% bandwidth filter corrected at 101.5 MHz.

For the uncorrected filters too, better agreement between FDT and FIT models is obtained by performing calculations at the upper band-edge frequency instead of the center frequency in the FIT model. Figure 16 shows the predicted response for the 2% bandwidth filter (uncorrected), with the FIT model calculated at 103.5 MHz. The agreement is clearly better than in Figure 13b where the FIT model was calculated at 100 MHz.

Figures 17a, 17b, and 17c compare the FIT and FDT models for a 5% bandwidth filter corrected at 3 different frequencies (100, 105, and 107.5 MHz). Obvious improvement is obtained by correcting at higher than center frequency.

Filters with wider bandwidths are not discussed since diffraction errors are known to be negligible with unapodized wideband filters [8]. This is because the convolution functions S(f) and D(f) [Eq. (26)] are narrowband functions (Figure 12) that go down rapidly at higher frequencies.

We thus conclude that for unapodized devices,

(1) The FIT model can be used to predict frequency response

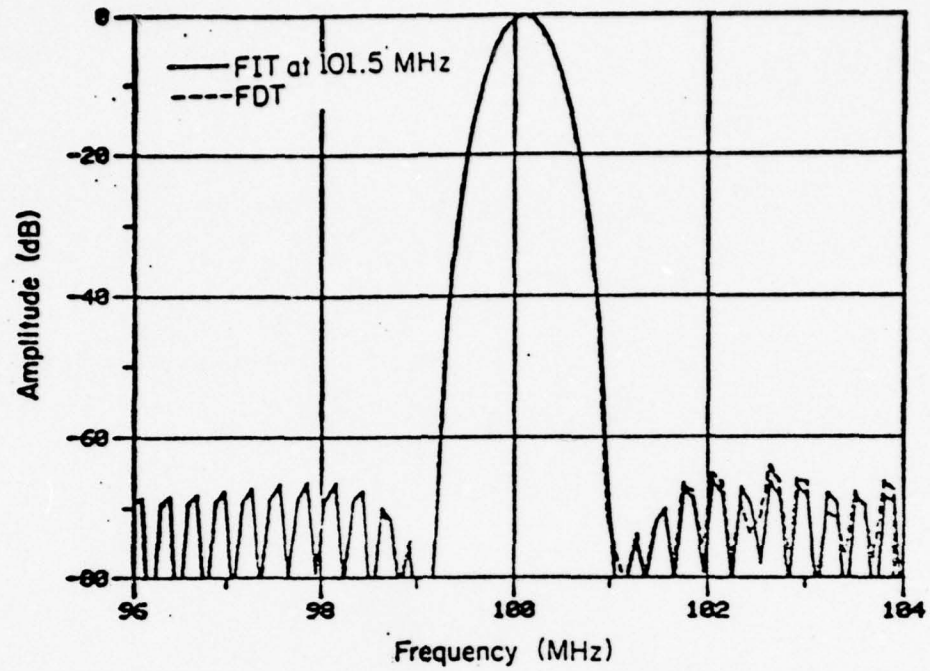

(a)

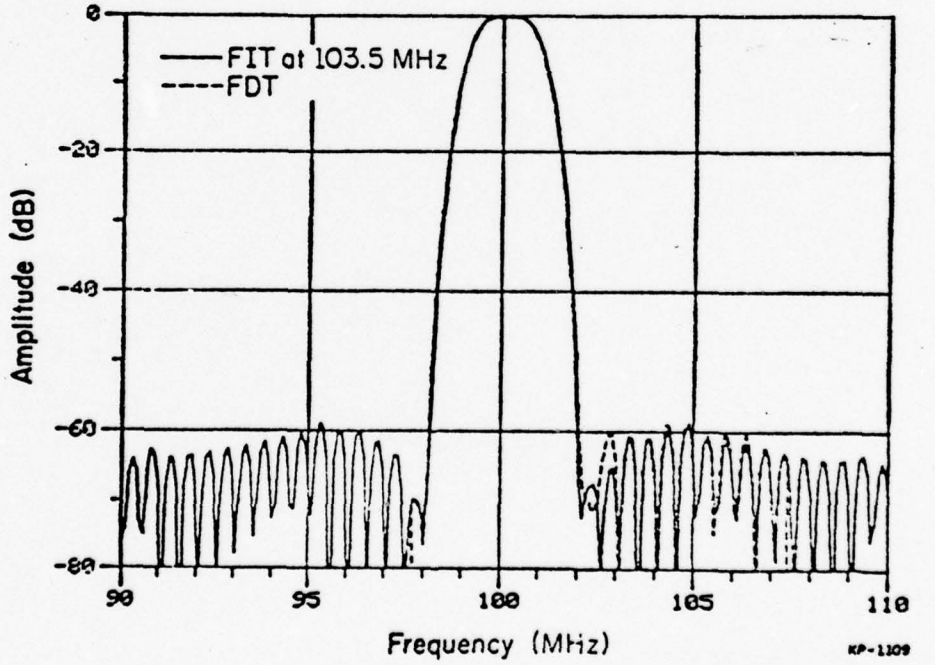

(b)

Figure 15. Response with diffraction calculated from the FDT model and the FIT model (at band-edge frequency) for unapodized
(a) 1% bandwidth filter corrected at 101.5 MHz.
(b) 2% bandwidth filter corrected at 103.5 MHz.

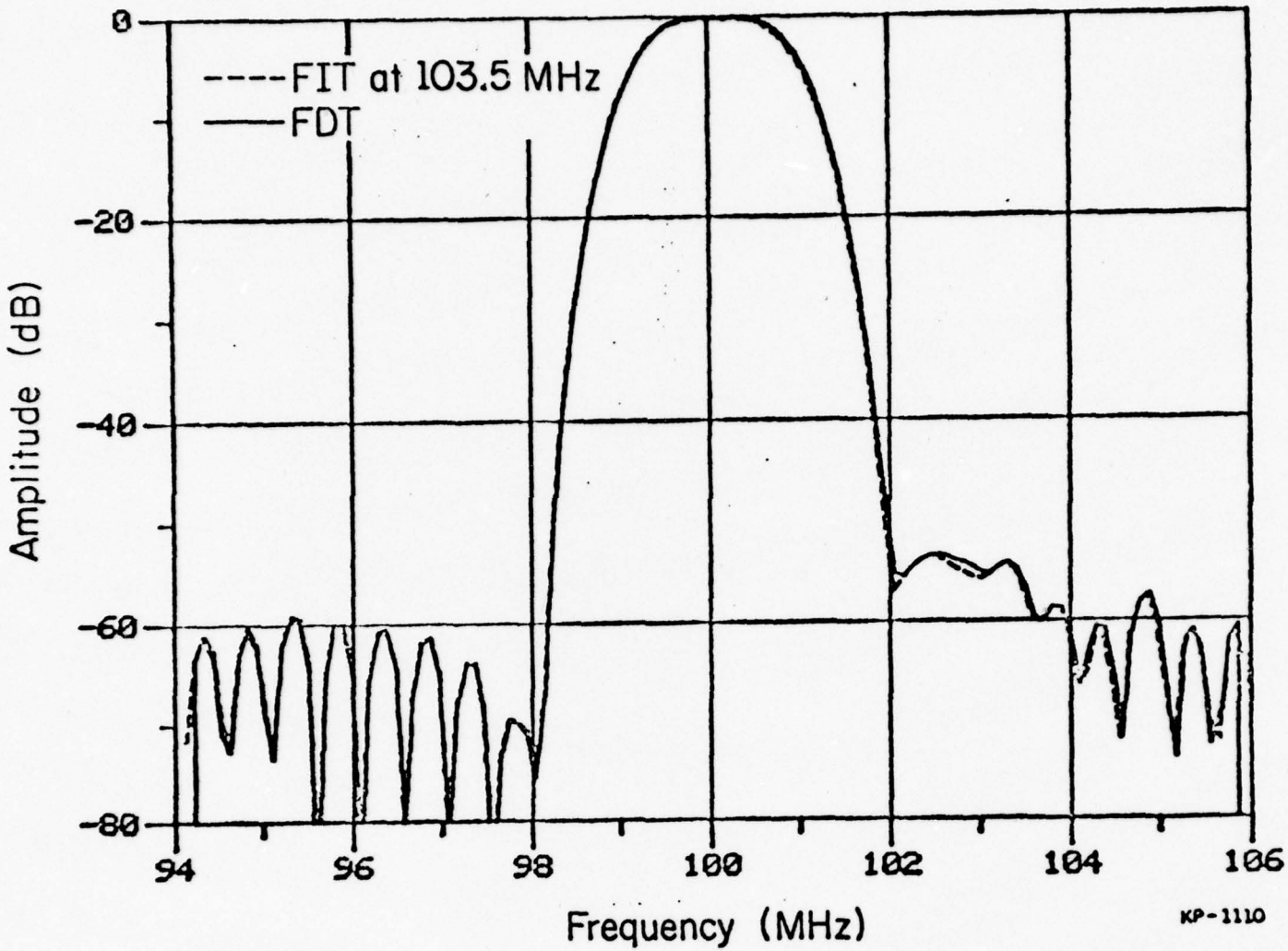

Figure 16. Response with diffraction for 2% bandwidth uncorrected unapodized filter calculated from the FDT and the FIT model (at 103.5 MHz).

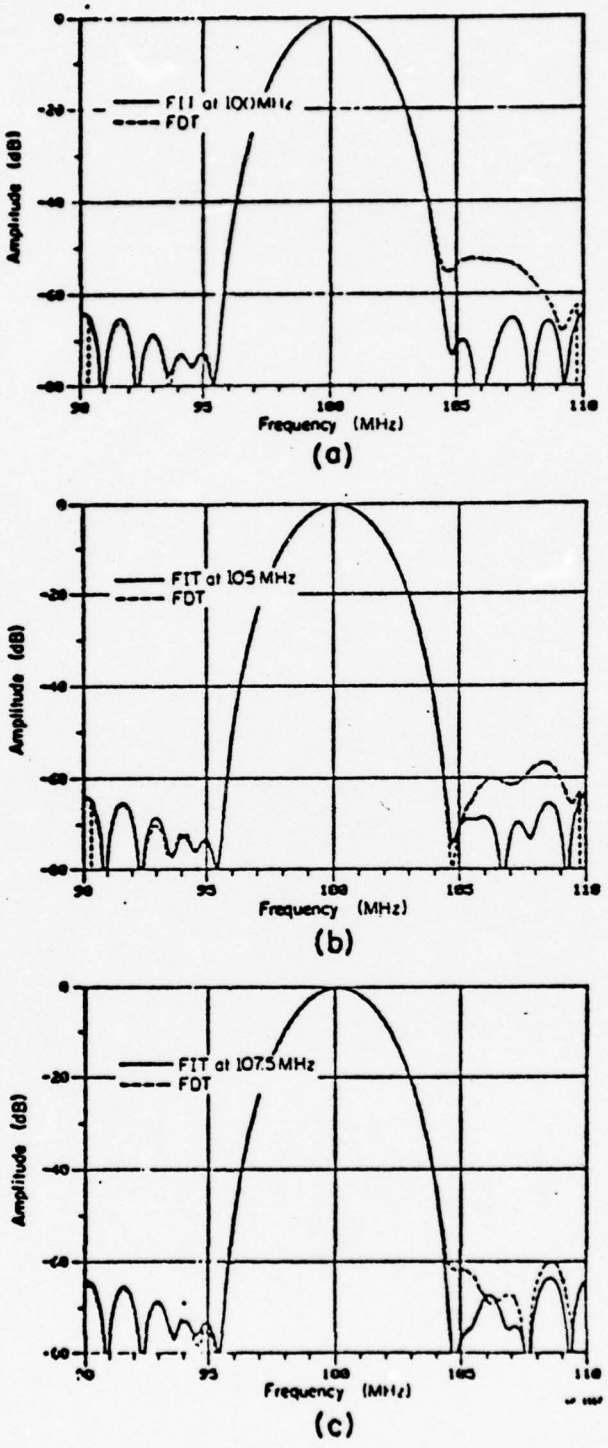

Figure 17. Response with diffraction calculated from the FDT and FIT model for unapodized 5% bandwidth filter corrected at
(a) 100 MHz
(b) 105 MHz
(c) 107.5 Mhz.

accurately down to 60 db or less by a judicious choice of f_0.

(2) Significant diffraction correction is obtained by correcting not at center frequency but around the band-edge frequency.

(b) Apodized Devices

For an apodized transducer the received signal at any finger is written as (from Eq. (2)),

$$U_R(f,t_n) = R(\hat{L},\ \rho(t_n)\cdot\hat{L},\hat{z}) \tag{28a}$$

As derived in Eq. (18),

$$R(\hat{L},\ \rho(t_n)\cdot\hat{L},\hat{z}) = e^{-j2\pi\hat{z}}\cdot\sqrt{2}\cdot\hat{L}\cdot S(F,\rho(t_n))$$

Thus,
$$U_R(f,t_n) = e^{-j2\pi ft_n}\cdot\sqrt{2}\cdot\hat{L}\cdot S(F,\ \rho(t_n)) \tag{28b}$$

Comparing with Eq. (4b), the diffracted tap weights are written as

$$W_D(f,t_n) = \sqrt{2}\ \hat{L}\cdot S(F,\ \rho(t_n)) \tag{28c}$$

For small Δf, Eq. (28c) is expanded as,

$$W_D(f,t_n) = \sqrt{2}\ L_0\left[S(F_0,\rho(t_n)) + \frac{\Delta f}{f_0}\, S(F_0,\rho(t_n)) + D(F_0,\rho(t_n))\right] \tag{29a}$$

where
$$D(F,\rho) = F\cdot\frac{\partial S(F,\rho)}{\partial F} = 1/\sqrt{2\pi F}\cdot e^{-jF(1+\rho^2)/4}\sin F\rho/2$$

For uncorrected apodized transducers the diffraction errors are around 30 db or less and the difference between the FIT and FDT models is not

perceptible (Figure 9a). However, the difference shows up for corrected devices. For a corrected device, we choose $\rho(t_n)$ such that $S(F_0, \rho(t_n)) = W(t_n)$ so that,

$$W_D(f,t_n) = \cdot \sqrt{2}\ L_0 \cdot W(t_n)\left[1 + \frac{\Delta f}{f_0} \frac{W(t_n) + D(F_0, \rho(t_n))}{W(t_n)}\right] \qquad (29b)$$

Thus the frequency response with diffraction is written as,

$$H_D(f) = \sum_{n=1}^{N} W_D(f,t_n)\, e^{-j2\pi f t_n}$$

$$= H(f) + \frac{\Delta f}{f_0} \cdot H(f) * B(f) \qquad (29c)$$

where

$$B(f) = \sum_{n=1}^{N} \frac{W(t_n) + D(F_0, \rho(t_n))}{W(t_n)} \cdot e^{-j2\pi f t_n}$$

Equation (29c) is of the same form as Eq. (27b) for unapodized devices. Both B(f) and C(f) represent the errors that cannot be corrected away for the respective cases.

However, it is not possible to obtain B(f) without specifying the apodization function $\rho(t_n)$. For comparison we have chosen a triangular apodization function $\rho(t_n)$ and obtained the corresponding B(f). This is compared with C(f) in Figure 18. It is noticed that B(f) is larger in magnitude than C(f). This is because of larger errors in the smaller taps in apodized devices; the fundamental limit to diffraction correction is thus higher for apodized devices than for unapodized devices.

This is shown in Figure 19 for a corrected apodized filter with 2% bandwidth. Correction is good only to about 50 db. An apodized device

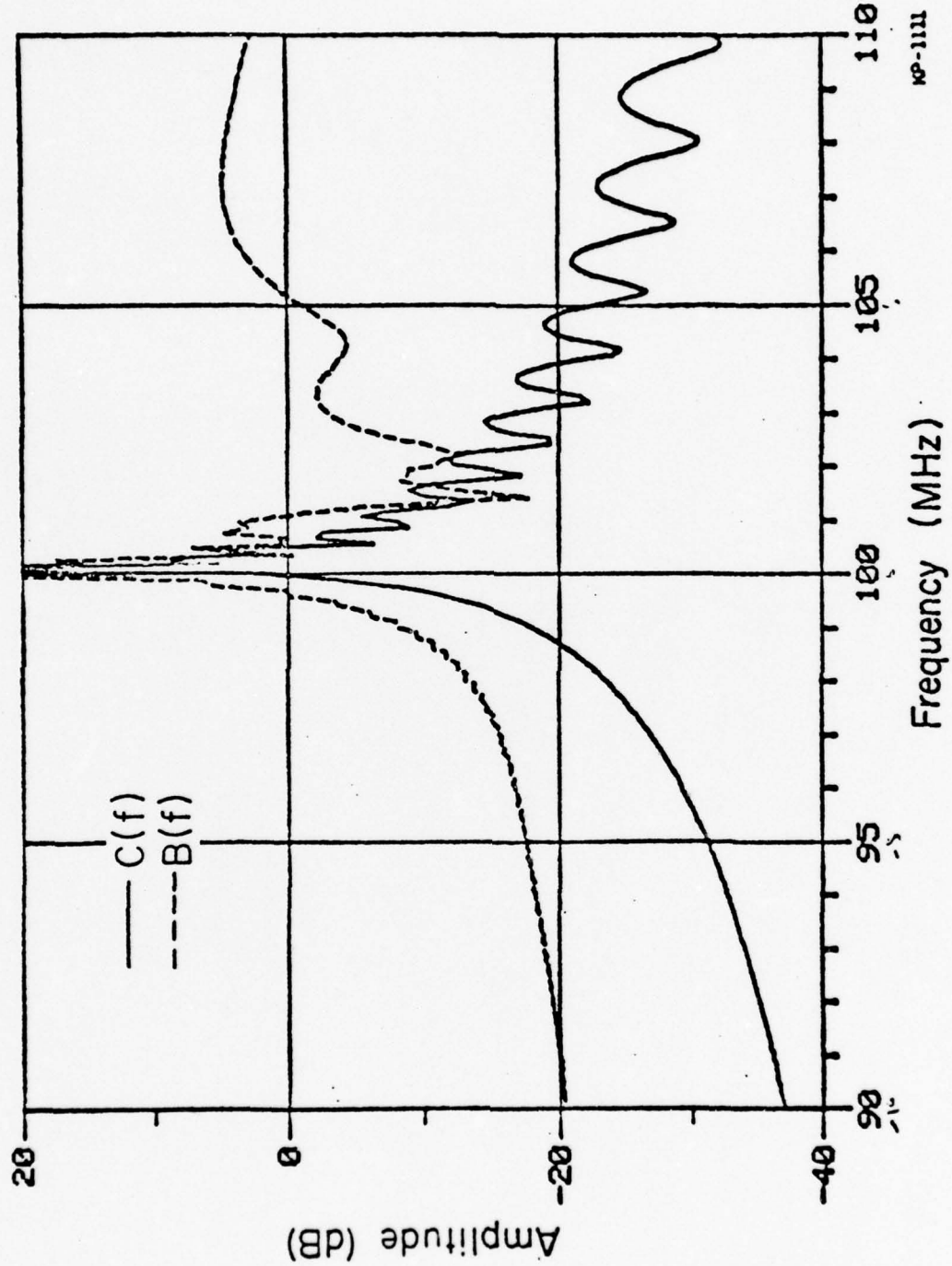

Figure 18. Comparing C(f) with B(f).

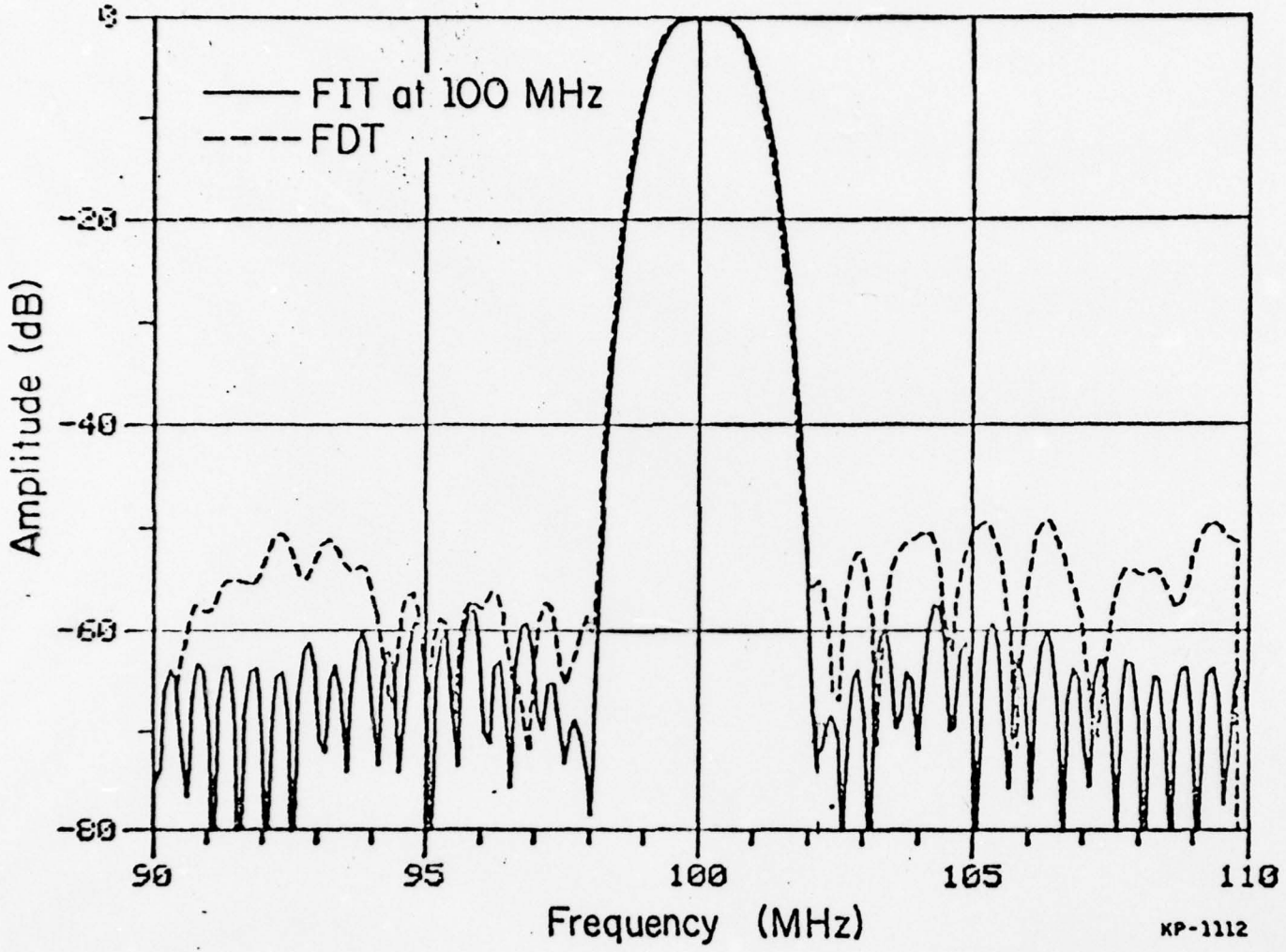

Figure 19. Response with diffraction for 2% bandwidth apodized filter corrected at 100 MHz, calculated from the FDT and the FIT model at 100 MHz.

with the best diffraction correction is still only about as good as an uncorrected unapodized device (Figure 13b).

Since for the apodized transducer the errors are spread over all frequency, the frequency of correction cannot be shifted for better results as in the unapodized case. In addition because of the broadband nature of B(f), diffraction errors tend to increase with wideband devices. This is in contrast to unapodized transducers where wideband devices have minimal diffraction errors due to the narrowband nature of C(f).

Figures 20a, 20b, and 20c compare the FIT and FDT models for different filters corrected at center frequency. It is clear that diffraction correction ceases to be effective for wide bandwidth filters with steep skirts.

We then conclude that there is a fundamental limit on the performance of SAW filters in the presence of diffraction. The results may be summarized as follows:

(1) Rejection levels below 60 db may be octained for unapodized filters by calculating the correcting diffraction effects at a frequency around the high side of the pass-band rather than at center frequency. The FIT model may similarly be used for analysis by performing the calculations at upper band-edge frequency.

(2) For uncorrected apodized filters the diffraction error level is ~30 db. At this level the FIT model may be used for analysis without significant error.

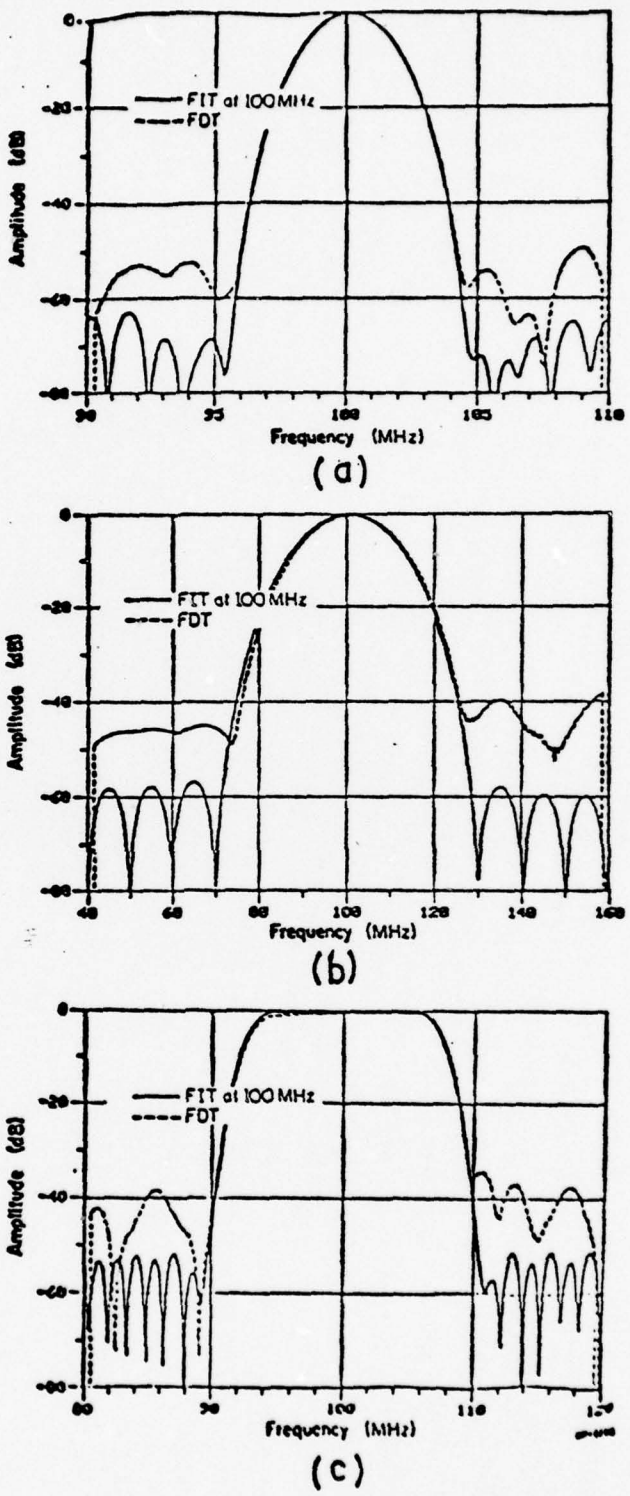

Figure 20. Response with diffraction for corrected apodized filters of varying bandwidths and selectivity calculated from the FDT and the FIT model at 100 MHz.

(3) The optimum correction for apodized filters may vary from ~50 db to ~35 db depending on the bandwidth and selectivity of the filter. However the optimum performance of an apodized filter will usually be worse than the performance of the corresponding unapodized filter without any correction.

Practical techniques for implementing diffraction correction using the FIT model are discussed in the next section.

2. Techniques for Tap Weight and Delay Correction

As discussed in Chapter I, Section 4, the tap weight with diffraction is related to the no diffraction tap weight by,

$$W_D = W \cdot E(F, \rho)$$

where $$E(F, \rho) = R(\hat{L}, \rho\hat{L}, \hat{z})/\rho e^{-j2\pi\hat{z}}$$

Given an ideal impulse response function $h(t_n)$, the FIT model is used to derive an impulse response function $h'(t_n)$ such that at some convenient frequency,

$$h(t_n) = h'(t_n) \cdot E(F(t_n), \rho(t_n)) \tag{30}$$

The function $h'(t_n)$ has to be determined by an iterative procedure. Single filters i.e., filters with a short input transducer and a weighted output transducer are assumed. For cascaded filters the problem is more complex since an individual tap cannot be identified with a particular value of t_n. The filter is then designed using $h'(t_n)$ as the impulse response. With diffraction this filter yields the ideal impulse response $h(t_n)$ at the chosen frequency. This design thus represents the best possible diffraction correction.

In general $h'(t_n)$ is a complex function, and this presents implementation problems. Szabo and Slobodnik showed [7] that for certain special filters the phase of $h'(t_n)$ may be ignored. However, for most practical filters this is not possible and a technique of implementing complex tap weights is needed in order to obtain significant improvement in performance.

There are three possible techniques to achieve complex tap weights:

(a) Tap Offset Along Propagation Path

Let h' be given by

$$h' = \rho e^{j\alpha} \tag{31}$$

where ρ and α are real numbers. This may be implemented by making the overlap equal to ρ and shifting the tap along the propagation path by a distance $\frac{\alpha}{2\pi} \cdot \lambda$ where λ is the wavelength at center frequency (or the frequency of correction).

Evidently this technique requires non-uniform tap-spacing. This creates problems with mask fabrication since most computer plotters move in discrete steps. Moreover, due to tap-interaction large offsets may change the effective tap weight.

(b) Tap Offset Perpendicular to Propagation Path

Tap delays may be adjusted within limits by shifting the position of the tap perpendicular to the propagation path i.e., by adjusting x (Figure 21). With larger offsets the contributing rays from the transmitter are more oblique and hence have larger delays.

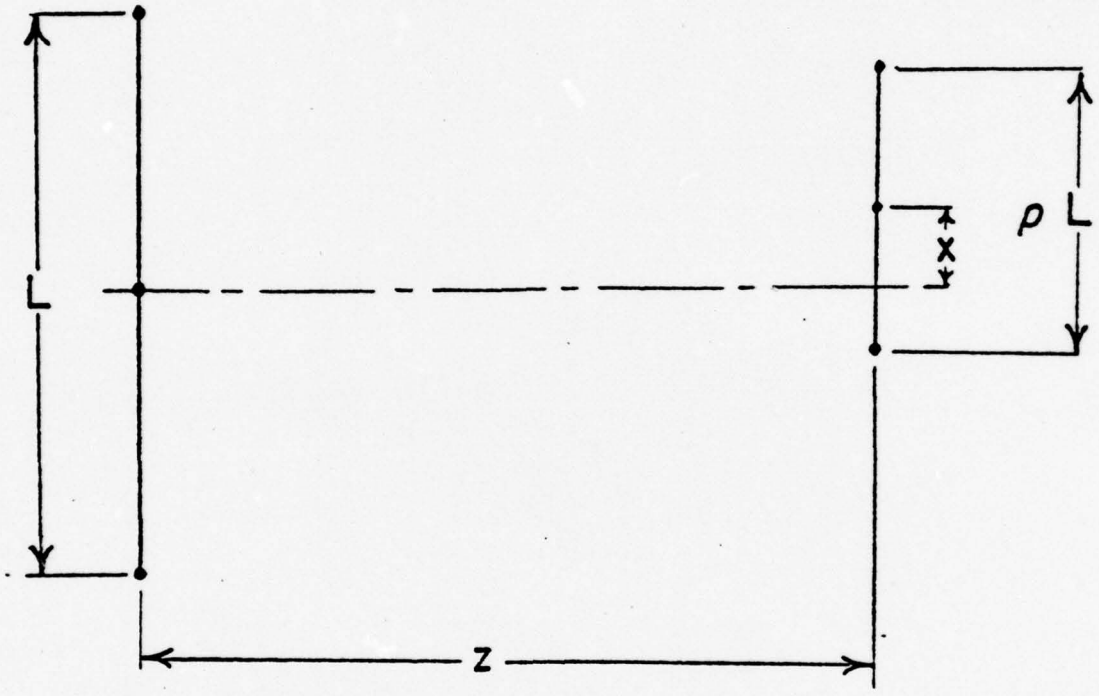

Figure 21. Parallel transmitter and receiver of unequal width with receiver offset from center.

Figures 22a and 22b show the amplitude and phase variation as a function of $\alpha = x/L$ for $\rho = 1.0$ and for two values of $F(= \pi\hat{L}^2/\hat{z}(1+\gamma))$. Figures 23a and 23b show the same for $\rho = .3$. It is seen that in the far field ($F = .5$) tap delays may be adjusted independent (almost) of tap weights by changing α. However, in the near field ($F = 50$) both tap weight and delay vary arbitrarily with α so that no simple design procedure can be devised.

(c) In-Phase and Quadrature Taps

In this technique each tap is replaced by an inphase and a quadrature tap spaced a quarter wavelength apart. The inphase tap has a weight of $\rho \cos \alpha$ and the quadrature tap has a weight $\rho \sin \alpha$ (ρ and α defined in Eq. (31)). The combined weight, W_T of the two taps at center frequency is given by

$$W_T = \rho \cos \alpha + \rho \sin \alpha \cdot e^{j\pi/2}$$

$$= \rho e^{j\alpha}$$

This technique thus yields the desired tap weight as expressed in Eq. (31).

Since the taps are uniformly spaced, this technique is free from the problems discussed earlier. There is no loss of resolution since most practical filters use equal length double fingers in order to suppress mechanical reflections.

In the next section experimental results are presented for a device built using this technique to implement diffraction correction.

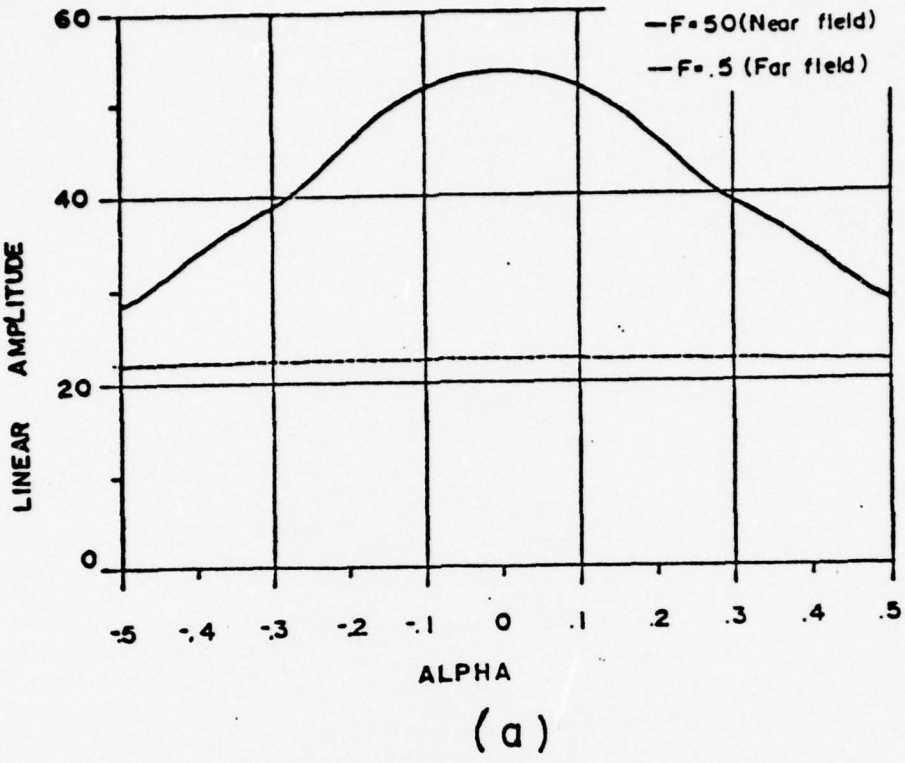

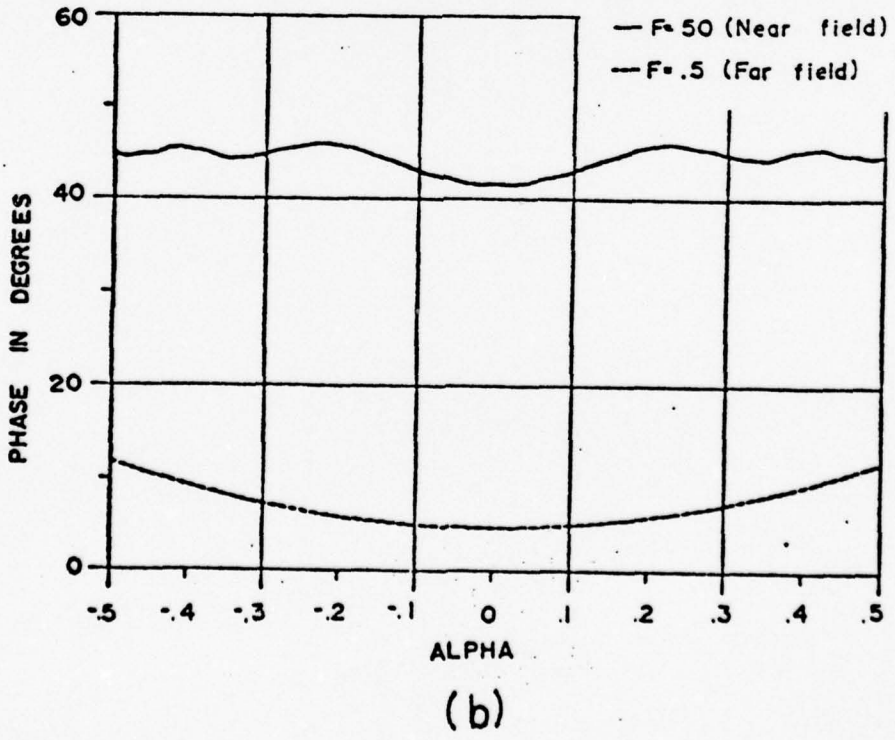

Figure 22. Amplitude and phase of received signal as a function of receiver offset for two values of F. (ρ = 1).
(a) Amplitude (b) Phase

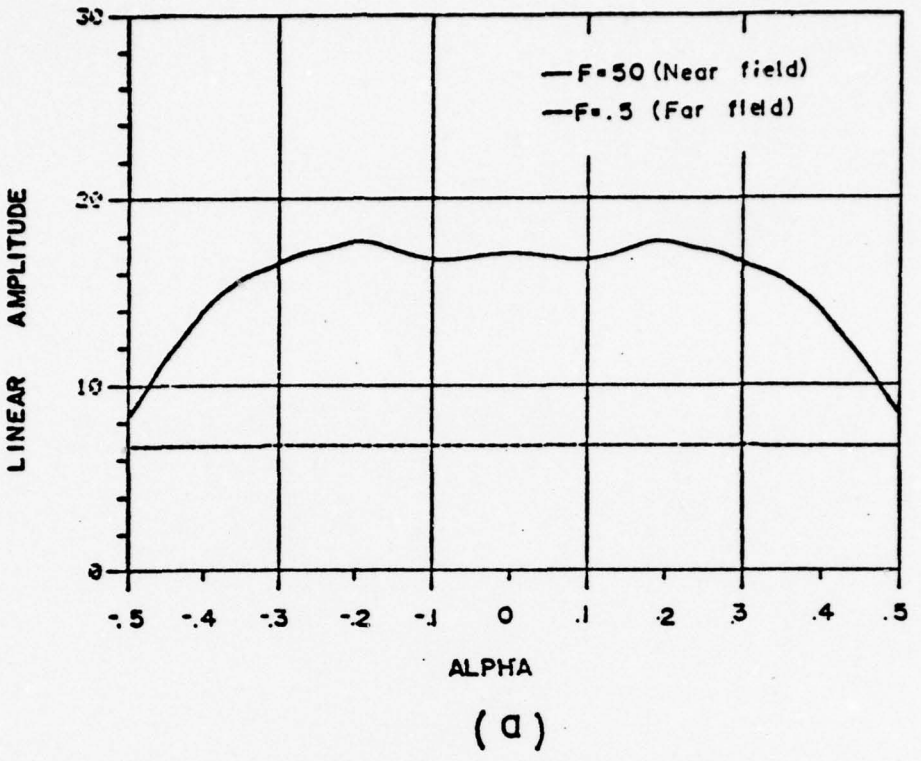

(a)

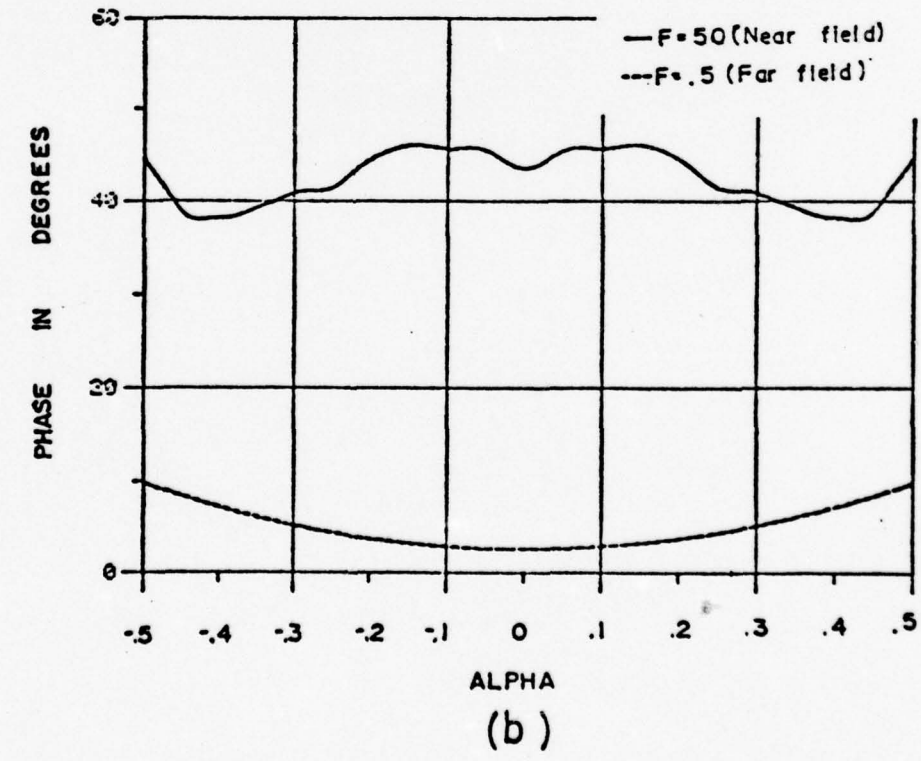

(b)

Figure 23. Amplitude and phase of received signal as a function of receiver offset for two values of F. (ρ = .3).
(a) Amplitude (b) Phase

3. Experimental Results

The filter considered in this section has a short uniform input transducer and an apodized weighted output transducer 200 wavelengths long. The maximum width of the transducers in 45 wavelengths and the center to center distance between the transducers is 190 wavelengths. The center frequency is 70 MHz and the bandwidth is about 1%. The substrate material is ST cut quartz.

Figure 24 shows the predicted frequency response including diffraction effects for the uncorrected filter. Using the method discussed in Section 2 (Eq. (30)) a corrected impulse response $h'(t_n)$ is calculated. As discussed earlier, $h'(t_n)$ has complex values with both amplitude and phase. Neglecting the phase gives rise to tap-delay errors. Figure 25 shows the predicted response with diffraction for a filter designed using $|h'(t_n)|$ as the impulse response.

Using inphase and quadrature taps $h'(t_n)$ is implemented both in magnitude and phase. Figure 26 shows the predicted and experimental results for a device built using this technique. (The predicted response also accounts for end-effect errors which were not corrected in the design.) Comparing with Figures 24 and 25 it is clear that significant improvement is obtained in the transition regions. However, there are significant errors in the experimental response especially on the high frequency side. The reasons for the spurious response is not clear yet. There are four possible reasons:

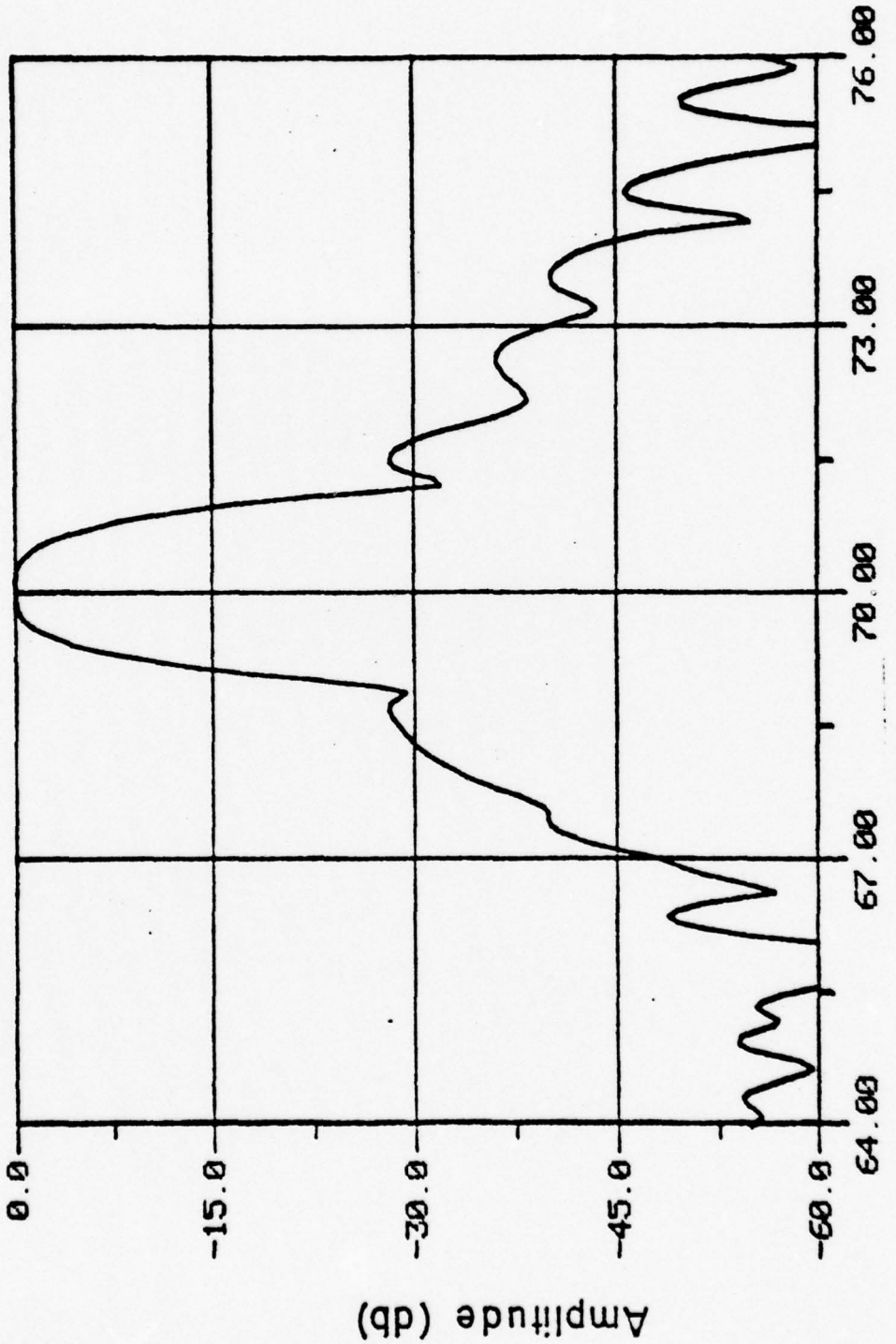

Figure 24. Predicted response with diffraction for uncorrected apodized filter.

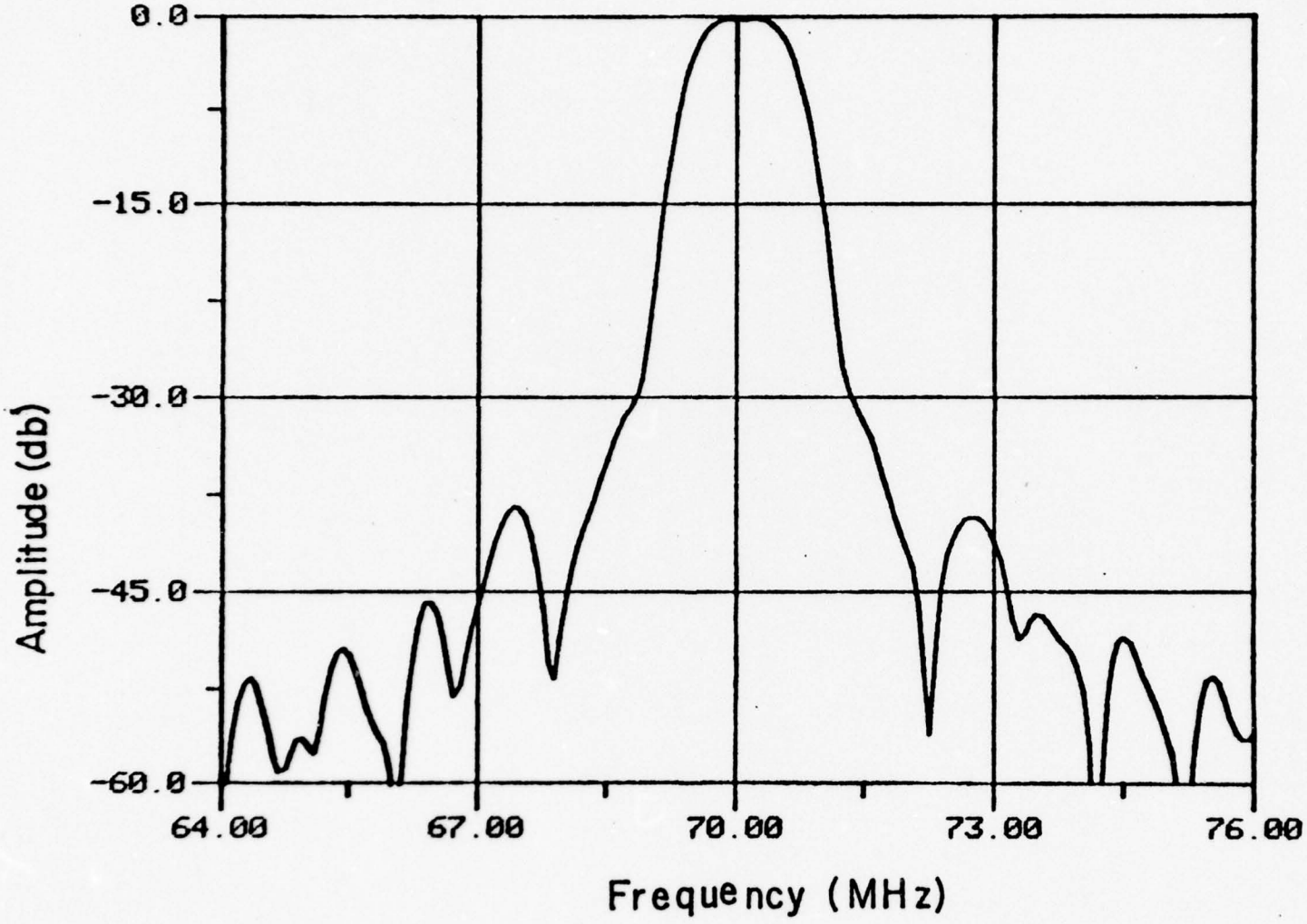

Figure 25. Predicted response with diffraction for a filter with only tap weight correction (without tap-delay correction).

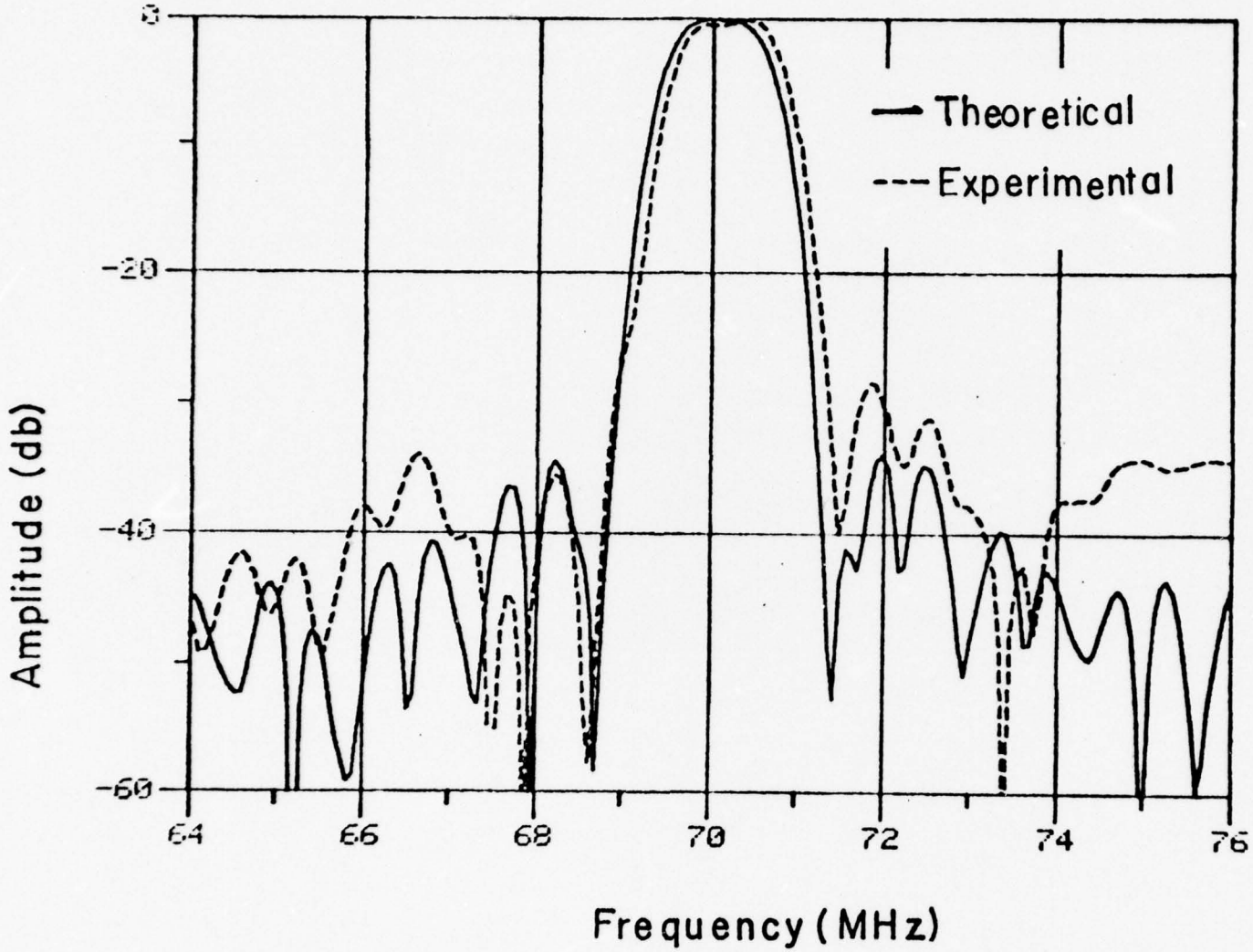

Figure 26. Predicted and experimental response for corrected filter with inphase and quadrature taps.

(1) Interaction between different taps caused by unequal length double fingers.

(2) Increased coupling to spurious modes because of the long output transducer.

(3) Effects of fringing fields on the small quadrature taps.

(4) Errors in crystal alignment.

The experimental frequency response is inverse Fourier transformed to yield the impulse response shown in Figure 27. It is apparent that there is a large tap-weight error at the center of the main lobe. A second device built using a different mask has the same error in the impulse response; which shows that it is not a fabrication error. It is possibly because of a spurious mode response superposed on the surface wave.

4. Concluding Remarks

In this chapter the design of single filters with diffraction-compensation is discussed. The limitations imposed by the frequency dependence of diffraction errors is investigated for apodized and unapodized filters. A practical implementation of diffraction-correction with inphase and quadrature taps is presented with experimental results.

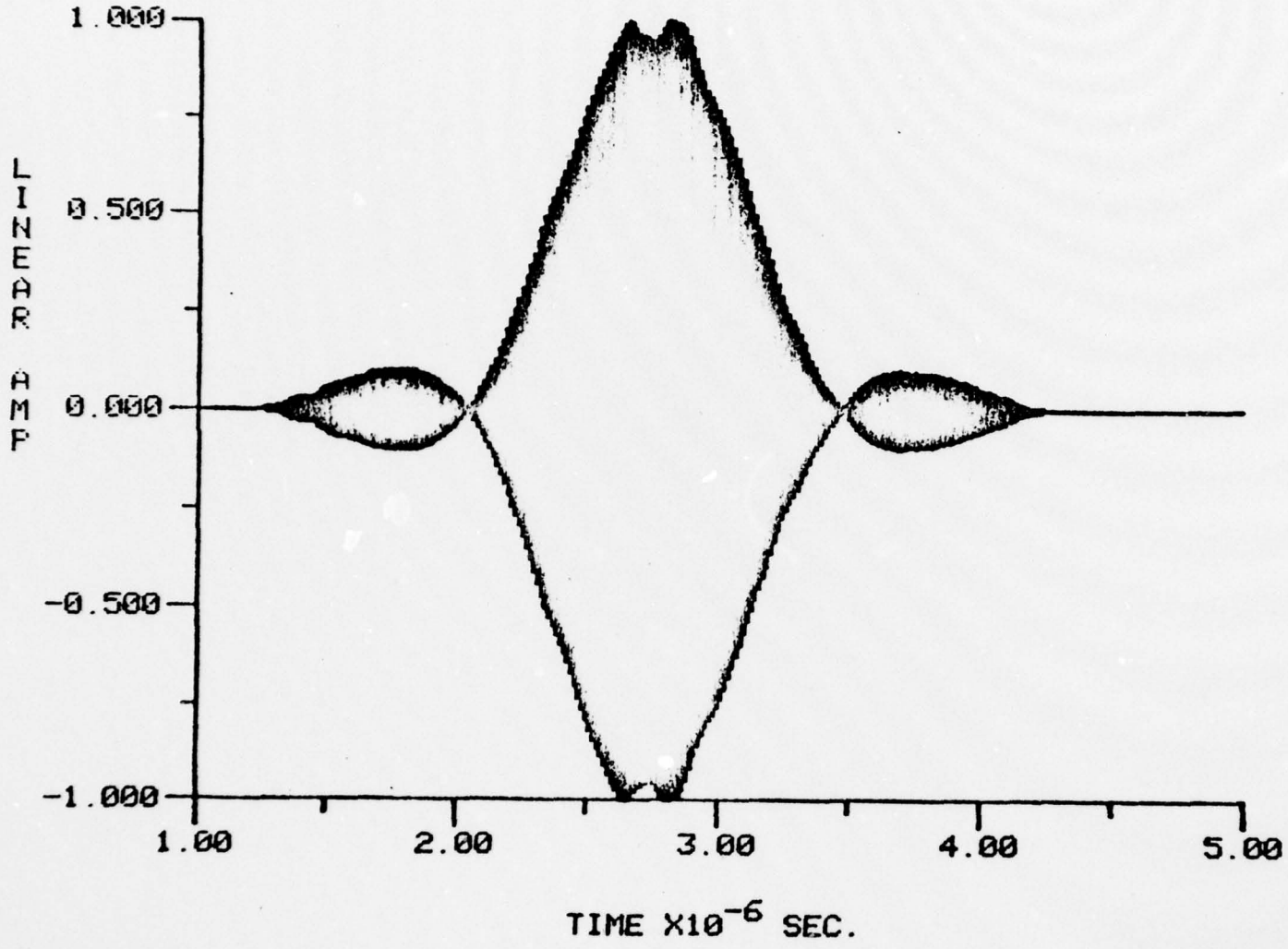

Figure 27. Impulse response of experimental device obtained by transforming experimental frequency response.

CHAPTER III: CASCADED FILTERS

In the last chapter the techniques of diffraction compensation were discussed for single filters where the input transducer is short (with only one electrode pair) and uniform. In practice for high-rejection filters it is often necessary to have both transducers with many weighted electrodes. By cascading two transducers a given impulse response can be realized with a smaller dynamic range of tap weights on either transducer so that tap weight errors are less. Moreover, both transducers being frequency selective, there is greater suppression of spurious modes.

In cascaded filters the taps on either transducer cannot be associated with any unique sample of the composite impulse response (i.e. with any unique time delay). The correction techniques discussed in the last chapter are thus not directly applicable.

Figure 28 shows two transducers with tap weight functions $W_1(t)$ and $W_2(t)$ separated by a center to center time delay of t_0. The composite impulse response is written as,

$$h(t) = \sum_{\tau} \Re(W_1(\tau),\ W_2(t-t_0-\tau),\ t) \qquad (32)$$

where the function $\Re$ represents the transfer function between the transmitter tap of weight W_1 and the receiver tap of weight W_2 separated by a time delay t. The exact form of the function will depend on the tap weighting technique.

In cascaded filters one transducer must be unapodized. Two apodized transducers cannot be cascaded, in general to produce a useful filter. The

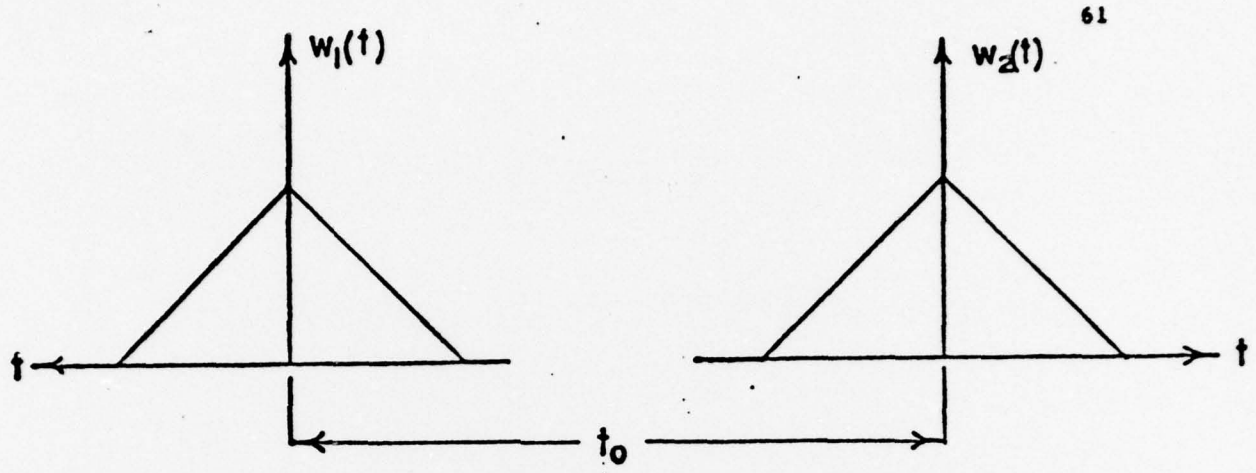

Figure 28. Two transducers operating in cascade.

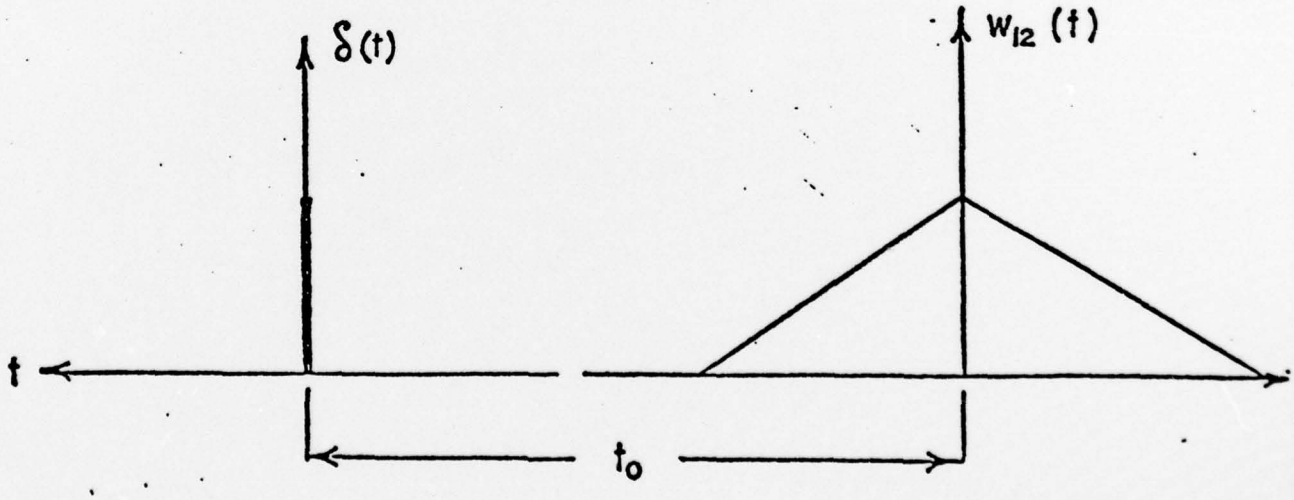

Figure 29. Equivalent single filter for cascaded unapodized transducers.

reasons are discussed briefly at the end of the chapter. It is assumed that the input transducer (w_1) is unapodized while the output transducer (w_2) may be apodized or unapodized.

In the absence of diffraction the function $\Re$ is written as,

$$\Re(w_1(\tau),\ w_2(t-t_0-\tau),\ t) = w_1(\tau)\cdot\ w_2(t-t_0-\tau)$$

From Eq. (32),

$$h(t) = \sum_{\tau} w_1(\tau)\ w_2(t-t_0-\tau) \tag{33}$$

so that the composite impulse response is just the convolution of $w_1(t)$ and $w_2(t)$ delayed by t_0. In this case,

$$H(\omega) = W_1(\omega)\cdot W_2(\omega)\cdot e^{-jwt_0} \tag{34}$$

where

$$H(\omega) = \sum_{t} h(t)e^{-j\omega t}$$

$$W_1(\omega) = \sum_{t} w_1(t)e^{-j\omega t}$$

$$W_2(\omega) = \sum_{t} w_2(t)e^{-j\omega t}$$

The design procedure is thus quite straightforward in the absence of diffraction. With diffraction, the function $\Re$ is more complicated and the problem is to obtain the functions $w_1(t)$ and $w_2(t)$ so that Eq. (32) yields the desired impulse response $h(t)$. In this discussion the frequency dependence of diffraction errors is neglected. The accuracy of correction is thus limited by the accuracy of the FIT model as discussed earlier. Two cases are considered separately; (1) when the output transducer is unapodized and (2) when the output transducer is apodized. The input transducer is assumed unapodized.

Both Transducers Unapodized

In this case the function $\hat{R}$ is written as

$$\hat{R}(w_1(\tau),\ w_2(t-t_0-\tau),t) = w_1(\tau) \cdot w_2(t-t_0-\tau) \cdot S(t)$$

where S(t) represents the diffraction error which depends only on the time delay between the transmitter tap and the receiver tap. Equation (32) is written as:

$$\begin{aligned} h(t) &= \sum_{\tau} w_1(\tau) \cdot w_2(t-t_0-\tau) \cdot S(t) \\ &= S(t) \cdot \sum_{\tau} w_1(\tau) \cdot w_2(t-t_0-\tau) \\ &= S(t) \cdot w_{12}(t) \end{aligned} \qquad (35)$$

where $w_{12}(t)$ denotes the convolution product of $w_1(t)$ and $w_2(t)$ delayed by t_0.

It is apparent from Eq. (35) that in this case the composite impulse response with diffraction is the same as if the input transducer has a single finger and the output transducer has a tap weight function given by $w_{12}(t)$ as shown in Figure 29. This equivalence of the cascaded filter to a single filter makes all the results of Chapter 2 applicable in principle. Diffraction correction can thus be carried out quite easily. The filter of Figure 29 is corrected to obtain a modified tap weight function $w_{12}'(t)$ using the methods discussed in Chapter 2. The individual tap weights of the two transducers $w_1'(t)$ and $w_2'(t)$ are now determined to satisfy the relationship:

$$w_1'(t) * w_2'(t) = w_{12}'(t)$$

Thus utilizing the equivalent single filter approach, diffraction errors are corrected in a straightforward manner (within the limitations of the FIT model).

An alternative approximate method of correction seems reasonable. In this method the tap weights on the output transducer are corrected with respect to a single finger at the center of the input transducer; and the tap weights on the input transducer are corrected with respect to a single finger at the center of the output transducer. It is interesting that this approximate approach yields no improvement over the uncorrected filter. To obtain significant correction the technique discussed earlier is used. The results for an example filter with identical input and output transducers each having about 800 taps, are shown in Figure 30.

. One Transducer Unapodized and the Other Apodized

In this case the function $\hat{R}$ is written as,

$$\hat{R}(w_1(\tau),\ w_2(t-t_0-\tau),t) = w_1(\tau)\cdot w_2(t-t_0-\tau)\cdot E(w_2(t-t_0-\tau),t)$$

where $E(w_2(t-t_0-\tau),t)$ is the diffraction error which depends on the receiver tap weight and the time delay between the transmitter and receiver taps.

Equation (32) is written as,

$$h(t) = \sum_{\tau} w_1(\tau)\cdot w_2(t-t_0-\tau)\cdot E(w_2(t-t_0-\tau),t) \qquad (36)$$

Since the error term in Eq. (36) cannot be taken out of the summation, there is no simple equivalence to a single filter as in the previous case.

This makes the problem of correction computationally more difficult. Given an impulse response $h(t)$, Eq. (36) has to be solved to yield the tap weight w_1 and w_2 for the two transducers. This requires an iterative optimization procedure.

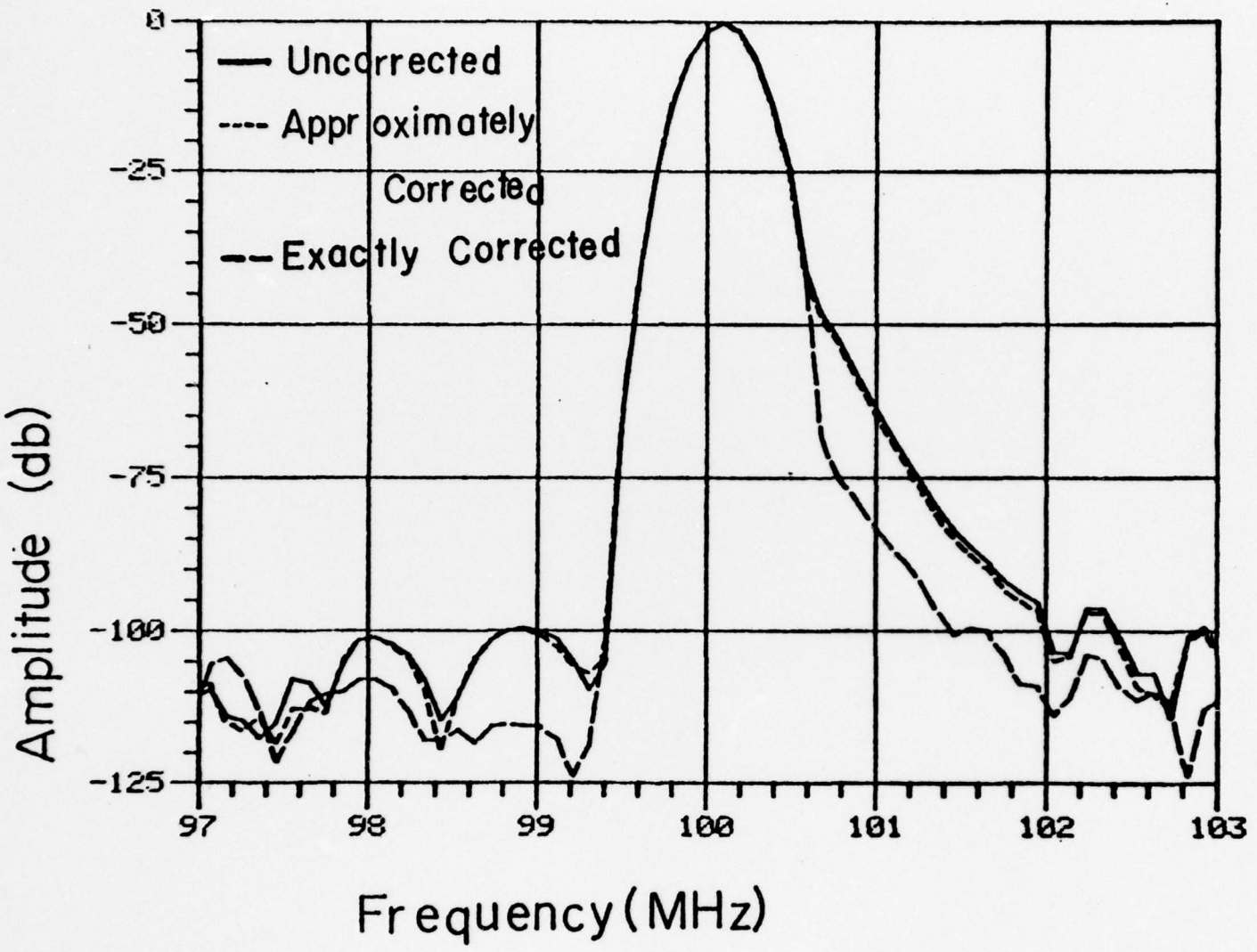

Figure 30. Predicted response with diffraction for a corrected, approximately corrected and an exactly corrected filter with both transducers unapodized.

An approximate approach may be adopted. $w_1(t)$ and $w_2(t)$ are first obtained for the no-diffraction case. A function $w_2'(t)$ is then obtained by correcting $w_2(t)$ with respect to a single finger at the center of the input transducer. $w_2'(t)$ is used as the tap weight function for the output transducer. The results expected from this approximate procedure are illustrated with an example.

A filter with 100 MHz as the center frequency and about 2% bandwidth is considered. The output transducer has 160 taps and is apodized weighted. The input transducer has 80 taps with a uniform tap weight of 1. Figure 31 shows the ideal frequency response without diffraction. Figure 32 shows the frequency response with diffraction for an uncorrected filter and a filter corrected approximately using the method discussed above. It is seen that the approximate approach yields significant improvement. For better results, a complicated optimization technique is required.

Figure 33 shows the predicted results for the filter considered in Figure 30, but with the output transducer apodized. In this case the approximate correction makes little improvement in the response. However, it is interesting to note that without any correction this filter has less error than in the last case when both transducers were unapodized. This is surprising since unapodized transducers acting singly have less diffraction errors than corresponding apodized transducers.

Cascaded Apodized Transducers:

Apodized transducers in general cannot be cascaded. Without diffraction, the function $\Re$(Eq.(32)) in this case is of the form

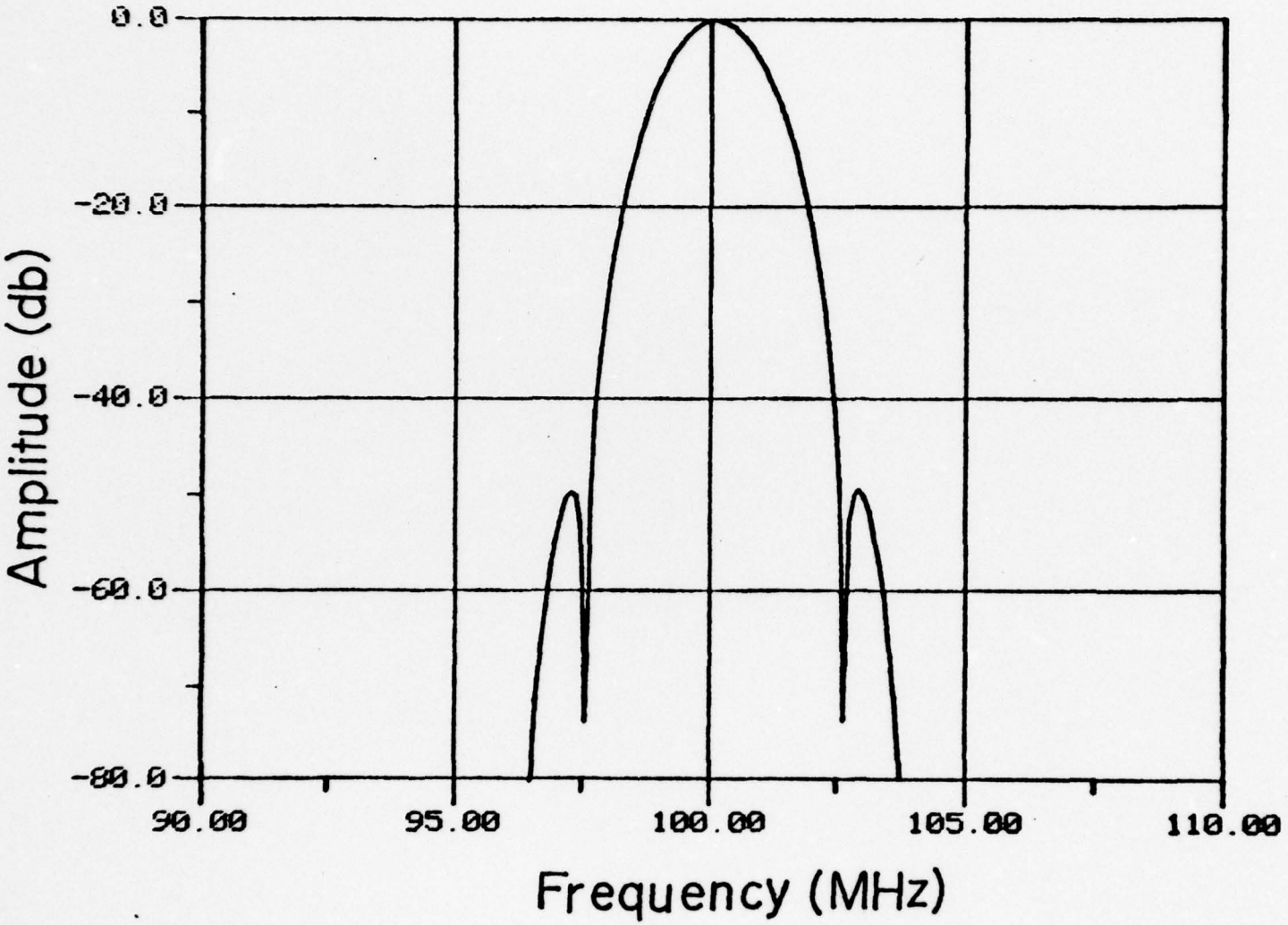

Figure 31. Specified frequency response for a cascaded filter with uniform input transducer and apodized output transducer.

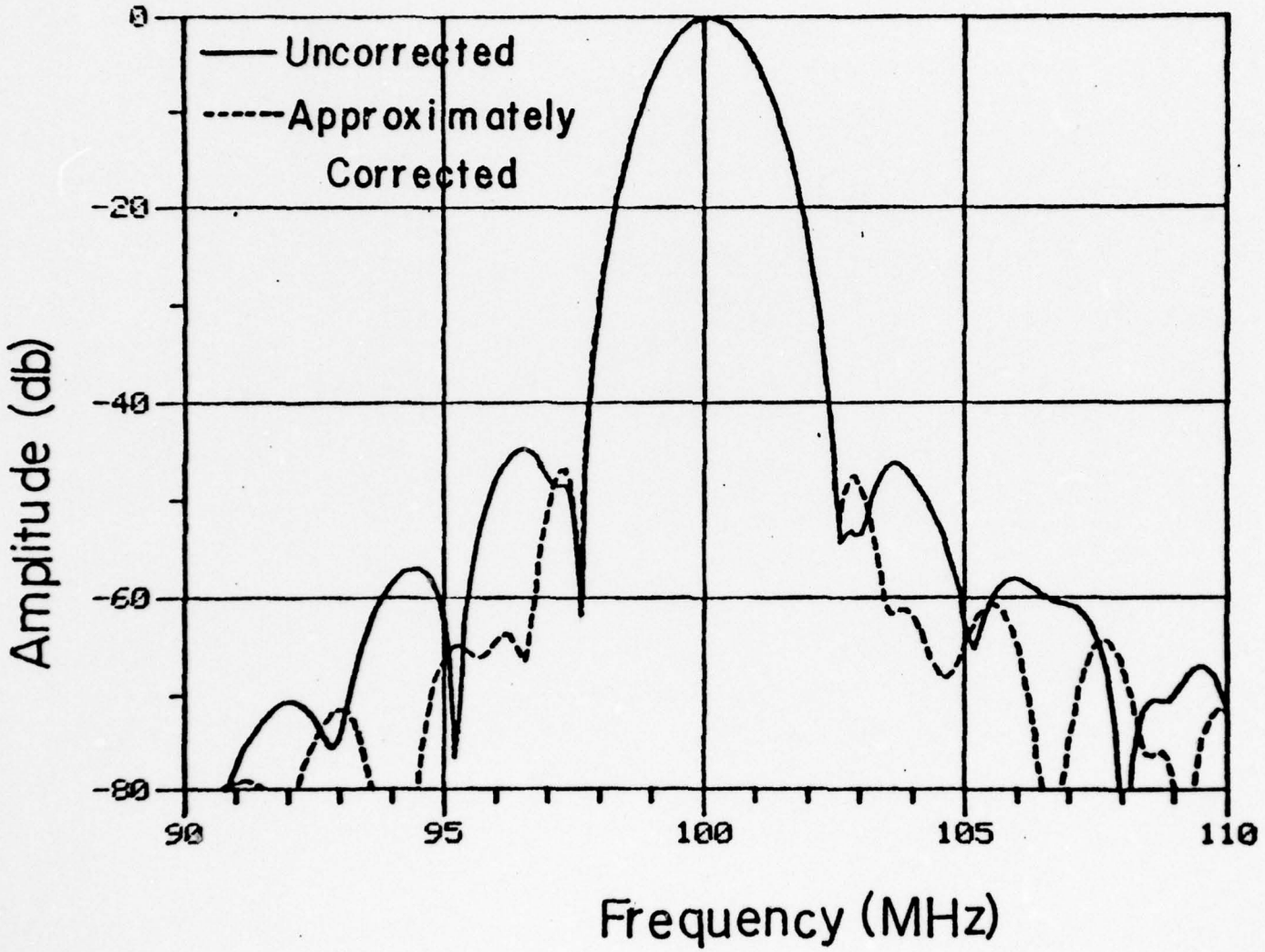

Figure 32. Predicted response with diffraction for uncorrected filter and approximately corrected filter.

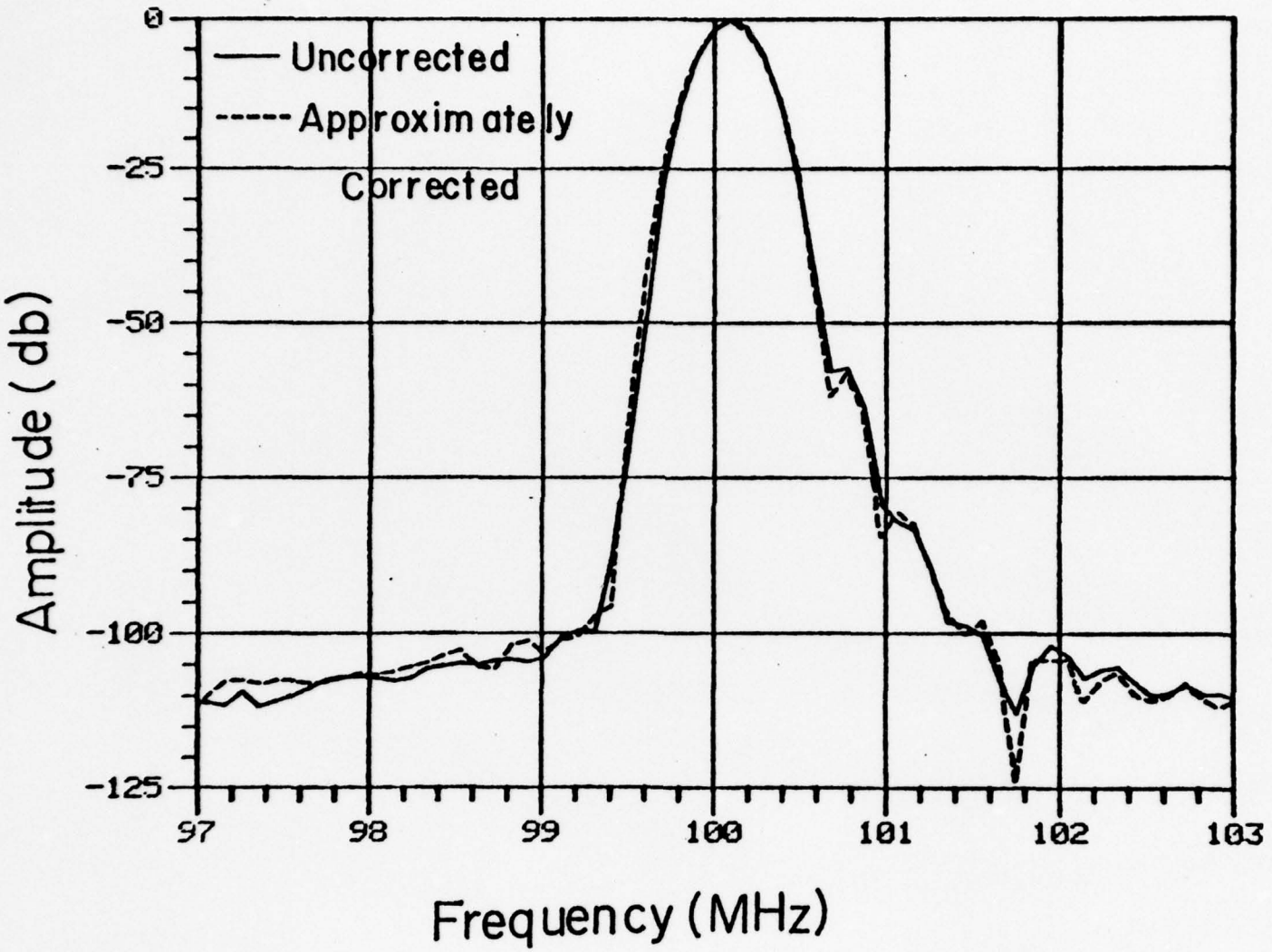

Figure 33. Predicted response with diffraction for a corrected and an approximately corrected filter with one transducer unapodized and the other apodized.

$$\hat{R}(w_1(\tau),\ w_2(t-t_0-\tau),t) = \min(w_1(\tau),\ w_2(t-t_0-\tau))$$

i.e., the resulting tap weight is equal to the smaller of the two taps. Thus,

$$h(t) = \sum_{\tau} \min(w_1(\tau),\ w_2(t-t_0-\tau))$$

It is not in general possible to find $w_1(t)$ and $w_2(t)$ to yield any arbitrarily specified $h(t)$. Thus even without diffraction the tap weights $w_1(t)$ and $w_2(t)$ cannot be designed to yield a useful impulse response.

Conclusions:

In this chapter the techniques of diffraction correction (based on the FIT model) as applied to cascaded filters have been discussed briefly. It has been shown that when both transducers are unapodized the problem may be treated in terms of an equivalent single filter, and the correction techniques developed for single filters may be applied with simple modifications. When one of the transducers is apodized, exact correction requires a complex iterative technique. An approximate correction based on the single filter approach may be used to yield significant improvement in performance.

REFERENCES

1. C. S. Hartmann et al., "Impulse Model Design of Acoustic Surface Wave Filters," IEEE Transactions, Vol. SU-20, No. 2, April 1973.

2. B. J. Hunsinger and R. Kansy, "SAW Filter Sampling Techniques," IEEE Transactions and Ultrasonics, SU-22, No. 4, July 1975, pp. 270-273.

3. D. Malocha and B. J. Hunsinger, "Capacitive Weighted Tap SAW Transducers," 1975 Ultrasonics Proceedings IEEE Cat. #75 CHO 994-45U, pp. 411-413.

4. C. S. Hartmann, "Weighting Interdigital Surface Wave Transducers by Selective Withdrawal of Electrodes," 1973 Ultrasonics Symposium.

5. B. J. Hunsinger et al., "Low Resolution Weighted Tap Transducers with Reflection and Diffraction Suppression," 1975 Ultrasonics Symposium.

6. Mitchell and Stevens, "Diffraction Effect in Small-Aperture Acoustic Surface Wave Filters," Wave Electronics, 1 (1974), pp. 201-218.

7. T. L. Szabo and A. J. Slobodnik, "Diffraction Compensation in Periodic Apodized Acoustic Surface Wave Filters," IEEE Transactions on Sonics and Ultrasonics, Vol. 21, No. 2, April 1974.

8. R. S. Wagers, "Diffraction Effects in Long Narrow ID Transducers," Proceedings IEEE 1975 Ultrasonics Symposium. R. S. Wagers, "SAW Diffraction Analysis by Paired Echo Superposition," IEEE Transactions on Sonic and Ultrasonics, SU-23, No. 4, July 1976.

9. T. L. Szabo and A. J. Slobodnik, "The Effect of Diffraction on the Design of Acoustic Surface Wave Devices," IEEE Transactions on Sonics and Ultrasonics, SU-20, 1973, pp. 240-251.

10. M. S. Kharusi and G. W. Farnell, "Diffraction and Beam Steering for Surface Wave Combined Structures on Anisotropic Substrates," IEEE Transactions on Sonics and Ultrasonics, SU-18, 1971, pp. 35.

11. M. S. Kharusi and G. W. Farnell, "On Diffraction and Focusing in Anisotropic Crystals," Proc. IEEE, 1972, pp. 945-956.

12. I. M. Mason and E. A. Ash, "Acoustic Surface Wave Beam Diffraction on Anisotropic Substrates," J. Appl. Phys. 42, 1971, pp. 5343.

13. I. M. Mason, "Anisotropy, Diffraction Scaling, Surface Wave Lenses and Focussing," J. Acoustic Soc. Am., 53, 1973, pp. 1123-28.

14. R. D. Weglein, M. R. Pedinoff, and H. Winston, "Diffracting Spreading of Surface Waves on $LiNbO_3$," Electronics Letters 6, 1970, pp. 654.

15. M. G. Cohen, "Optical Study of Ultrasonic Diffraction and Focussing in Anisotropic Media," J. Appl. Phys. 38, 1967, pp. 1123-1128.

16. J. C. Grable, J. D. Maines, N. R. Ogg, "Surface-Wave Diffraction on $LiNbO_3$," Electronics Letters 7, 1971, pp. 253-255.

17. N. R. Ogg, "A Huygens' Principle for Anisotropic Media," J. Phys. A.: Gen. Phys. 4, 1971, pp. 382-388.

18. J. D. Maines, G. L. Moule, and N. R. Ogg, "Correction of Diffraction Errors in Acoustic Surface Wave Pulse Compression Filters," Electronics Letters 8, 1972, pp. 431.

19. P. J. Hagon and K. M. Lakin, "The Influence of Near Field Diffraction on SAW Device Performance," Proc. IEEE Ultrasonics Symposium, 1974, pp. 341-344.

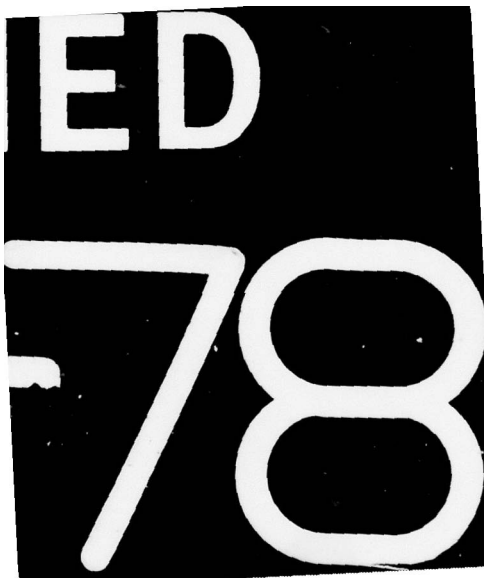
ED
78